The influence of particle concentration and composition on the fractionation of 210 Po and 210 Pb along the North Atlantic GEOTRACES transect GA03

Yi Tang, Gillian Stewart, Phoebe J. Lam, Sylvain Rigaud, Thomas Church

1 **The influence of particle concentration and composition on the fractionation of ^{210}Po and**

2 **^{210}Pb along the North Atlantic GEOTRACES transect GA03**

3

4 Yi Tang[a,b], Gillian Stewart[b,a,*], Phoebe J. Lam[c], Sylvain Rigaud[d,e], Thomas Church[d]

5 [a] Department of Earth and Environmental Sciences, the Graduate Center, City University of New

6 York, New York, NY 10016, USA

7 [b] School of Earth and Environmental Sciences, Queens College, City University of New York,

8 Flushing, NY 11367, USA

9 [c] Ocean Sciences Department, University of California Santa Cruz, Santa Cruz, CA 95064, USA

10 [d] School of Marine Science and Policy, University of Delaware, Newark, DE 19716, USA

11 [e] University of Nîmes, EA 7352 CHROME, rue du Dr. Georges Salan, 30021 Nimes, France

12

13 **Corresponding author: gstewart@qc.cuny.edu**

14

15 **Abstract**

16 　　The disequilibrium between ^{210}Po and ^{210}Pb has been used as a proxy for the particle flux

17 from the upper ocean. The particle concentration and composition effect on the partitioning

18 behavior of ^{210}Po and ^{210}Pb is, however, still unclear. Here, we investigate this association by

19 comparing dissolved (< 0.45 μm) and particulate (small: 1-51 μm; large: > 51 μm) ^{210}Po and

20 ^{210}Pb activity with size-fractionated major particle concentration and composition data from

21 the US GEOTRACES GA03 zonal transect cruises. We observed inverse relationships

22 between partition coefficients (K_d) for the radionuclides and the concentration of suspended

23 particulate matter (SPM) in the water column, known as the "particle concentration effect."

24 We examined the relationships between ^{210}Po, ^{210}Pb, and particle composition in the top

25 500m by using Pearson pairwise correlations for individual phases and principal components

26 analysis (PCA) for variations among multiple phases. In addition to these analyses, an end-

27 member mixing model was developed to estimate K_d for ^{210}Po and ^{210}Pb in the small

28 particulate size fraction from the compositional phases. The model predicted the range of

29 observed K_d(Pb) well, but was unable to predict the observed K_d(Po) as consistently, possibly

30 because of the bio-reactive nature of ^{210}Po. Despite this, we found a strong relationship

31 between ^{210}Po and both $CaCO_3$ and POM, as well as between ^{210}Pb and both opal and

32   lithogenic phases. All of our analyses demonstrated that the fractionation of ^{210}Po and ^{210}Pb

33   differed between the coast and open ocean along the GA03 transect.

34

37

38   **1. Introduction**

39   ^{210}Po ($T_{1/2}$ = 138.4 d) and ^{210}Pb ($T_{1/2}$ = 22.3 y) are particle-reactive radionuclides in the

40   ^{238}U decay series, produced through the decay of ^{222}Rn ($T_{1/2}$ = 3.8 d). The disequilibrium

41   between ^{210}Po and ^{210}Pb has been used in many studies to determine particle export from the

42   upper ocean (e.g. Buesseler et al., 2008; Friedrich and Rutgers van der Loeff, 2002; Murray

43   et al., 2005; Shimmield et al., 1995; Stewart et al., 2007a; Verdeny et al., 2008), in a similar

44   application to the more commonly used ^{234}Th/^{238}U system (e.g. Buesseler et al., 1992;

45   Charette et al., 2001; Cochran, 2003). However, the fluxes of particulate organic carbon

46   (POC) derived from these two techniques are often inconsistent and even contradictory

47   (Buesseler et al., 2008; Friedrich and Rutgers van der Loeff, 2002; Le Moigne et al., 2013;

48   Stewart et al., 2007a; Verdeny et al., 2008). For example, the POC fluxes derived from ^{234}Th

49   were higher than those derived from ^{210}Po in the Polar Front region, where diatoms were

50   dominant in the phytoplankton (Friedrich and Rutgers van der Loeff, 2002), while ^{210}Po-POC

51   flux was greater than the ^{234}Th-POC flux in the Sargasso Sea where small phytoplankton

52   such as *Prochlorococcus* and *Synechococcus* dominated the community (Bibby et al., 2008;

53   Buesseler et al., 2008). In addition, POC fluxes derived from ^{210}Po were usually higher than

54   ^{234}Th-derived estimates in the middle of gyres (e.g., Sargasso Sea, and Hawaii), whereas the

55   opposite was generally true near the margins (Stewart et al., 2007a; Verdeny et al., 2009).

56   The greatest inherent differences between ^{210}Po/^{210}Pb and ^{234}Th/^{238}U have been

57   interpreted as a result of the different half-lives of ^{210}Po and ^{234}Th, and the different particle

58   affinities of the three particle-reactive radionuclides (^{210}Po, ^{210}Pb, ^{234}Th) (e.g. Murray et al.,

59   2005; Verdeny et al., 2009). In particular, for the ^{234}Th/^{238}U pair, only ^{234}Th is particle-

60   reactive while ^{238}U is highly soluble in seawater (Djogic et al., 1986). In contrast, in the

61   ^{210}Po/^{210}Pb technique, both radionuclides are particle-reactive although they have different

62   chemical behaviors: ^{210}Po generally has a higher affinity for particles than ^{210}Pb (Heyraud et

63   al., 1976; Kharkar et al., 1976). Furthermore, [210]Po and ^{210}Pb have different binding

64   preferences, with [210]Po associated with proteins and sulfur-containing compounds (Carvalho,

65   2011; Fisher et al., 1983; Larock et al., 1996; Stewart et al., 2007b; Stewart and Fisher,

66   2003), while ^{210}Pb is adsorbed onto particle surfaces and is associated with biogenic silica

67   and lithogenic particles (Bacon et al., 1976; Friedrich and Rutgers van der Loeff, 2002;

68   Shannon et al., 1970; Stewart et al., 2005).

69   Several studies have used field collected marine material to simulate the binding behavior

70   of Pb and Po radionuclides in the natural environment in the laboratory (Chuang et al., 2013;

71   2014; 2015; Yang et al., 2013). Evidence from these laboratory experiments suggests that

72   each radionuclide binds to specific biopolymeric functional groups, with enhanced

73   adsorption of [210]Po by proteins, while polysaccharides enhance the binding of [210]Pb (Quigley

74   et al., 2002; Yang et al., 2013), suggesting that [210]Po and ^{210}Pb could be fractionated by

75   specific organic and/or inorganic compounds during their sorption onto particles.

76   In this paper, we combined the measurements of [210]Po and ^{210}Pb in the dissolved and

77   particulate phases, and the major phase components of suspended particulate matter (SPM)

78   from the U.S. GEOTRACES North Atlantic transect. With these measurements, we

79   examined the role of particle concentration and composition in the scavenging and

80   fractionation of [210]Po and [210]Pb. The inter-correlations among the radionuclides and major

81   particle components have also been investigated, followed by principal component analysis

82   (PCA) aiming to reduce the number of variables to only those that are most significant in

83   describing the variability of the data set. We also applied end member mixing analysis

84   (EMMA (Li, 2005)) to estimate the scavenging intensities of [210]Po and ^{210}Pb for particles

85   with different compositions.

86   **2.   Methods**

87   **2.1. Sampling and analysis**

88   Seawater samples were collected at 7 "super" stations (with extra casts to provide large-

89   volume samples) from the R/V Knorr during the US GEOTRACES North Atlantic zonal

90   transect (NAZT), cruises KN199-04 and KN204-1. Cruise KN199-04 departed from Lisbon,

91   Portugal in October 2010 and ended in Cape Verde in November 2010. Cruise KN204-1

92   departed from Woods Hole, MA in October 2011 and ended in Cape Verde in December

93   2011 (Fig. 1). The super stations sampled included the three stations nearest to the coasts:

stn.10-1 off Lisbon and within the influence of the Mediterranean outflow, stn.10-9 located just west of the Mauritanian shelf break, and stn.11-1 off the New England continental shelf. The other four open ocean stations were mainly located in the North Atlantic subtropical gyre, including key stations 11-10 at the BATS site, and 11-16 at the TAG hydrothermal site.

Seawater samples (~ 20 L) were collected for dissolved ^{210}Po and ^{210}Pb analysis throughout the water column at each station (12-16 depths/station) by using 30 L Niskin bottles mounted on a standard CTD rosette sampler. Particulate ^{210}Po and ^{210}Pb samples were collected using McLane in situ pumps that had been modified to accommodate two filter heads (Cutter et al., 2010; Lam et al., 2015). The paired 51 μm polyester prefilters and 1 μm quartz fiber filters (Whatman QMA) were designed to simultaneously collect large size fraction (LSF, > 51 μm) and small size fraction (SSF, 1-51 μm) particles, respectively. Details on collection and analysis of water samples and particulate matter (both small and large particulate matter) for ^{210}Po and ^{210}Pb are given in Rigaud et al. (2015). The dissolved and particulate ^{210}Po and ^{210}Pb data is available at http://www.bco-dmo.org/dataset/3914 and http://www.bco-dmo.org/dataset/3917, respectively.
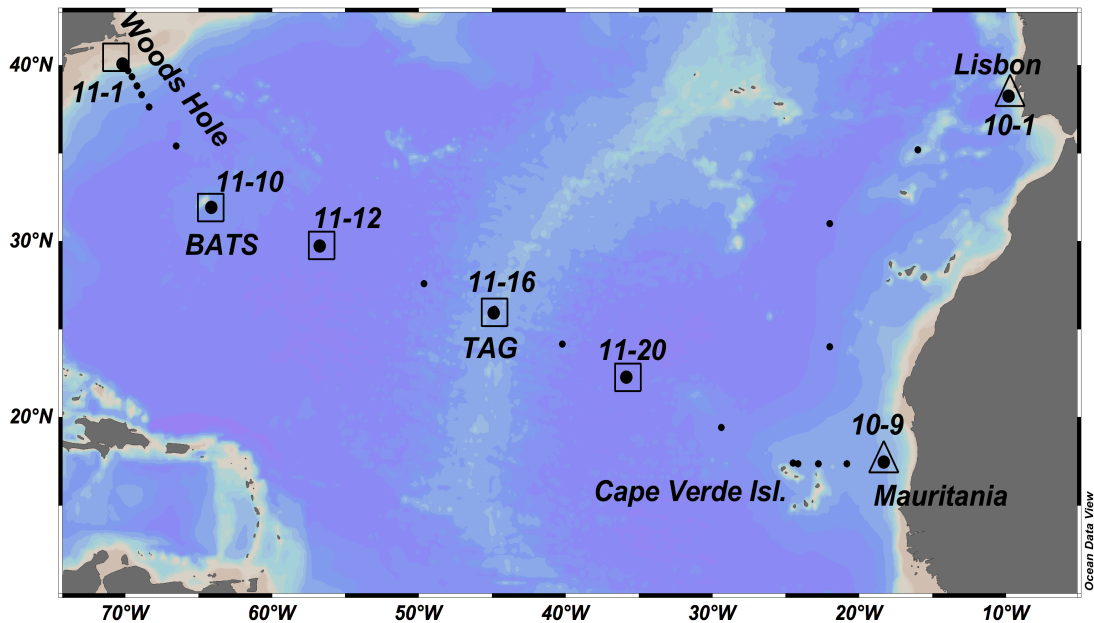

Fig. 1. Map showing stations along the US GEOTRACES GA03 North Atlantic zonal transect, from which samples were analyzed. Triangles and squares indicate stations from 2010 and 2011, respectively. BATS is the Bermuda Atlantic Time-series Site and TAG is the TAG hydrothermal site.

2.2. Size-fractionated particle composition and concentrations

The concentrations of six major particle compositional components (POC, $CaCO_3$, opal, lithogenic matter, iron, and manganese) in both the LSF and SSF at all seven stations along the transect were collected as part of the GEOTRACES NAZT project, along with basic physical and chemical parameters. The details on particle sampling and particle composition determination are described in Lam et al. (2015) and Ohnemus and Lam (2015). In addition, the mass of suspended particulate matter (SPM) was estimated as the sum of the chemical dry weight of the major particulate phases.

2.3. Composition correlation and PCA

The full dataset includes the activity of ^{210}Po and ^{210}Pb, and the concentration of six major phase particle components including POC, $CaCO_3$, opal, lithogenic matter, Fe, and Mn (Lam et al., 2015) in both SSF and LSF from the 7 "super" stations. The data matrix is grouped into 2 major areas: near the continental margins ("coastal" stns.10-1, 10-9 and 11-1), and in the open ocean (stns.11-10, 11-12, 11-16 and 11-20). Here we focus on the samples collected from the upper 500 m depth where biological activity and aerosol deposition play the most important roles in the fractionation of ^{210}Po and ^{210}Pb.

First, we used a Pearson pairwise correlation matrix to investigate how the size fractionated particulate ^{210}Po, ^{210}Pb related to the 6 major particle components. The significance of correlation coefficients, and strength of linear relationships between each pair of variables was determined by 2-tailed t-test at $p < 0.05$. To evaluate the correlation coefficient (r), we arbitrarily assign a "weak" correlation with correlation coefficient $|r| = 0.4$-0.49, a "moderate" correlation with $|r| = 0.5$-0.59, and a "strong" correlation with $|r| \geq 0.6$ in the following discussion.

We next analyzed interrelationships between particle composition measurements in the SSF and LSF using a principal component analysis (PCA) for the eight variables. We applied a transformation to the sample data prior to PCA by performing centering (mean subtraction) and scaling (dividing the centered columns by their standard deviations). While we examined the first three principal components of the PCA, the first two principal components alone captured > 65% of the total variance in each dataset so the results were further visualized using a biplot, which can provide inter-unit distance and indicate clustering of observations as well as display variances and correlations of the variables (Kohler and Luniak, 2005).

146   Third, we examined the information contained in the first three principal components by

147   regression of the principal component (PC) score of each observation against the

148   concentration of SPM, apparent oxygen utilization (AOU), and depth. If there was a

149   statistical relationship between PC scores and any of these parameters, we concluded that the

150   PC was reflective of that parameter regardless of the nature of the relationship. Because the

151   signs of PC scores are arbitrary and the data has been transformed, whether the relationship is

152   positive or negative, linear or non-linear has no significance to our interpretation.

153   **2.4. Partition Coefficients Analyses**

154   The partition coefficients (K_d) of [210]Po and ^{210}Pb are useful for describing their affinity to

155   marine particles (Bacon et al., 1976; Baskaran and Santschi, 1993; Wei and Murray, 1994).

156   The interpretation of the K_d(Po) is complicated because while ^{210}Pb only adsorbs to the

157   surface of particles, [210]Po is both sorbed to surfaces and also taken up into the cytoplasm of

158   phytoplankton cells and bioaccumulated through food chains (see Discussion for further

159   explanation). Even though the interactions of [210]Po and ^{210}Pb with particles are not the same,

160   we will use "adsorption" or "sorption" for both [210]Po and ^{210}Pb to describe their particle

161   association in this paper.

162   K_d (L kg^{-1}) is defined as:

$$K_d = \frac{A_p}{A_d} \times \frac{1}{SPM} \tag{1}$$

164   where A_p and A_d represent the nuclide activities in the particulate and the dissolved phases

165   (dpm 100L^{-1}), respectively, and SPM is the suspended particulate matter concentration (µg L^{-}

166   ^{1}). K_d provides a measure of the partitioning of radionuclides between the dissolved and

167   particulate phases. The conceptualized scavenging models consider chemical interactions

168   between radionuclides either (1) in the dissolved and total particulate phases (two-box

169   model) or (2) in the dissolved – small – large particulate phases (three-box model) or (3) in

170   the truly dissolved – colloidal – small – large particulate phases (Baskaran et al., 1992; Clegg

171   and Whitfield, 1991; 1990; Rigaud et al., 2015; Savoye et al., 2006). We calculated the

172   coefficients of the bulk partitioning between the dissolved and small particulate phases

173   (K_d_SSF), and between the dissolved and total particulate phases (K_d_TOT) without

174   considering colloidal phase due to lack of data. However, in our samples over 90% of the

175   total particulate radionuclide activity was in the small size fraction, and therefore these K_d

176   values were very similar. We will only present the K_d_SSF in this paper.

177   Next, we examined the degree to which [210]Po and ^{210}Pb are fractionated during sorption.

178   The fractionation factor (F), a ratio of the corresponding bulk K_d's (Chase et al., 2002;

179   Murray et al., 2005; Nozaki et al., 1998),

180       $F(Po/Pb) = K_d(Po)/K_d(Pb)$ (2)

181   was used to investigate the preferential sorption of [210]Po relative to [210]Pb.

182   Furthermore, in order to interpret the relationship between particle composition and the

183   bulk partition coefficients, a six-end-member mixing model was developed here similar to

184   the one published by Hayes et al. (2015) for thorium isotopes.

185       $K_d = \sum_1^6 (K_d)_i \cdot f_i = (K_d)_1 \cdot f_1 + (K_d)_2 \cdot f_2 + (K_d)_3 \cdot f_3 + (K_d)_4 \cdot f_4 + (K_d)_5 \cdot f_5 +$

186    $(K_d)_6 \cdot f_6$ (3)

187   where K_d is the observed bulk partition coefficient of a given nuclide, $(K_d)_i$ is the partition

188   coefficient for pure end member i, f_i is the proportion of end member i of the total mass of a

189   particle sample, where $i = 1$ (POM), 2 ($CaCO_3$), 3 (opal), 4 (lithogenic material), 5 (Fe), 6

190   (Mn). Eq. (1) and (3) were formatted for each particle sample, and therefore for a set of given

191    $i = n$ samples, f_i ($n \times 6$ matrix) and K_d^i ($n \times 1$ matrix) are all known. The unknown $(K_d)_i$

192   (6×1 matrix) can be solved by Eq. (4) using non-negative least squares regression (since the

193   negative K_d has no physical meaning).

194
$$\begin{bmatrix} f_1^1 & f_2^1 & f_3^1 & f_4^1 & f_5^1 & f_6^1 \\ f_1^2 & f_2^2 & f_3^2 & f_4^2 & f_5^2 & f_6^2 \\ f_1^3 & f_2^3 & f_3^3 & f_4^3 & f_5^3 & f_6^3 \\ & & \cdots & & & \end{bmatrix} \times \begin{bmatrix} (K_d)_1 \\ (K_d)_2 \\ (K_d)_3 \\ (K_d)_4 \\ (K_d)_5 \\ (K_d)_6 \end{bmatrix} = \begin{bmatrix} k_d^1 \\ k_d^2 \\ k_d^3 \\ \cdots \end{bmatrix} \qquad (4)$$

195   We estimated the standard error of the derived end-member K_d values using the jackknife

196   resampling technique (Efron and Stein, 1981). Finally, the derived end-member fractionation

197   factors, F(Po/Pb), were calculated from Eq. (2) for each compositional component.

198   **3. Results**

199   **3.1. Correlations**

200   In the open ocean, [210]Po activity was strongly correlated with POC and moderately

201   correlated with $CaCO_3$ in the small particles, and [210]Po activity in the large particles was

202   strongly correlated with $CaCO_3$, moderately correlated with opal, and weakly correlated with

203   POC (Table 1). [210]Pb activity in the open ocean, in contrast, was moderately correlated with

204   CaCO$_3$, opal, and Mn in the large particles but there were no significant correlations with

205   ^{210}Pb activity in the small particles. In the coastal waters, both ^{210}Po and ^{210}Pb activities in the

206   large particles were strongly correlated with POC, CaCO$_3$, and opal. ^{210}Po and ^{210}Pb activities

207   in the small particles near the coasts, however, had different relationships with the 6

208   particulate components relative to those in large particles. For instance, ^{210}Pb activity

209   strongly correlated with opal and Mn, and moderately correlated with lithogenic matter and

210   Fe near the coasts whereas ^{210}Po activity was found to be strongly correlated with lithogenic

211   matter and Fe.

212

213   Table 1. Pairwise Pearson Correlation Coefficients, r, within size-fractionated principal particle compositions in

214   the top 500 m at coastal (stns.10-1, 10-9 and 11-1) and open ocean (stns.11-10, -12, -16 and -20) stations. Bold

215   values with * and ** denote moderate and strong correlation with $p < 0.05$ by t-test, respectively.

	Coasts				Open Ocean			
	SSF (n = 19)		LSF (n = 18)		SSF (n = 20)		LSF (n = 19)	
	^{210}Po	^{210}Pb	^{210}Po	^{210}Pb	^{210}Po	^{210}Pb	^{210}Po	^{210}Pb
POC	0.05	0.07	**0.68****	**0.60****	**0.68****	0.30	0.45	0.18
CaCO$_3$	0.25	0.44	**0.72****	**0.65****	**0.59***	0.42	**0.71****	**0.59***
Opal	-0.01	**0.64****	**0.76****	**0.70****	0.18	-0.14	**0.53***	**0.50***
Litho	**0.75****	**0.54***	0.07	0.05	-0.06	-0.01	0.34	0.10
Fe	**0.74****	**0.56***	0.08	0.07	-0.03	0.00	0.15	-0.05
Mn	0.36	**0.84****	0.43	0.42	-0.47	-0.11	0.34	**0.58***

216

217   Overall, the correlations between the particle components and ^{210}Po and ^{210}Pb activity in

218   the large particles were reasonably consistent between coastal and open ocean samples,

219   whereas the corresponding correlations in the small particles varied between those two

220   oceanic provinces.

221   **3.2. Principal Component Analysis**

222   Principal component analysis (PCA) was applied to all eight measured variables to

223   identify a new set of fewer, uncorrelated variables that can explain a substantial portion of

224   the variation of the original variables. The new set of variables, also called the principal

225   components (PC), will result in a lower dimensional space that explains most of the variation.

226   We analyzed all the SSF data and all the LSF data as two datasets, and PCA results were

227   summarized in Table 2, including the loadings of the first three principal components (total 8

228   principal components) and their contribution in explaining of the total variance. In the SSF

229   dataset (Table 2, SSF), the first three principal components contained 76.9% of the variation

230   of the eight original variables, with 49.8% explained by PC1, 14.8% explained by PC2, and

231   12.3% explained by PC3. The highest loadings of PC1 were from Mn, Fe, $CaCO_3$ and

232   lithogenic matter, PC2's highest loadings were ^{210}Po and POC, whereas lithogenic matter and

233   Fe were most important to PC3 (Table 2, Fig. 2).

234

235   Table 2. The first three principal component loadings, percentage of variance explained by each principal

236   component, and their cumulative percentage of total variance in the small size fraction (SSF) and the large size

237   fraction (LSF) of the particles. The numbers in bold font indicate the absolute loadings that are higher than 0.4.

	Variables	PC1	PC2	PC3
SSF **(1-51 μm)**	^{210}Po	-0.001	**0.858**	0.070
	^{210}Pb	-0.226	0.118	-0.149
	POC	-0.279	**0.427**	-0.245
	$CaCO_3$	**-0.414**	0.056	-0.286
	Opal	**-0.401**	-0.205	**-0.406**
	Litho	**-0.412**	-0.023	**0.570**
	Fe	**-0.417**	-0.034	**0.553**
	Mn	**-0.441**	-0.146	-0.187
	% of Variance	49.8	14.8	12.3
	Cumulative %	49.8	64.6	76.9
LSF **(> 51 μm)**	^{210}Po	**-0.408**	-0.110	**0.466**
	^{210}Pb	-0.396	-0.070	**0.593**
	POC	-0.362	-0.292	**-0.493**
	$CaCO_3$	**-0.405**	-0.239	-0.324
	Opal	-0.386	-0.321	-0.121
	Litho	-0.243	**0.536**	-0.195
	Fe	-0.249	**0.532**	-0.163
	Mn	-0.334	**0.409**	0.058
	% of Variance	59.9	29.8	7.4
	Cumulative %	59.9	89.7	97.1

238

239   In contrast, the first three components of the LSF dataset explained 97.1% of the total

240   variance, in which PC1 explained 59.9%, PC2 explained 29.8%, and PC3 explained 7.4%

241   (Table 2, LSF). We observed that the highest PC1 loadings came from ^{210}Po and $CaCO_3$,

9

242   PC2's highest loadings were from lithogenic matter, Fe, and Mn, and PC3 loadings were

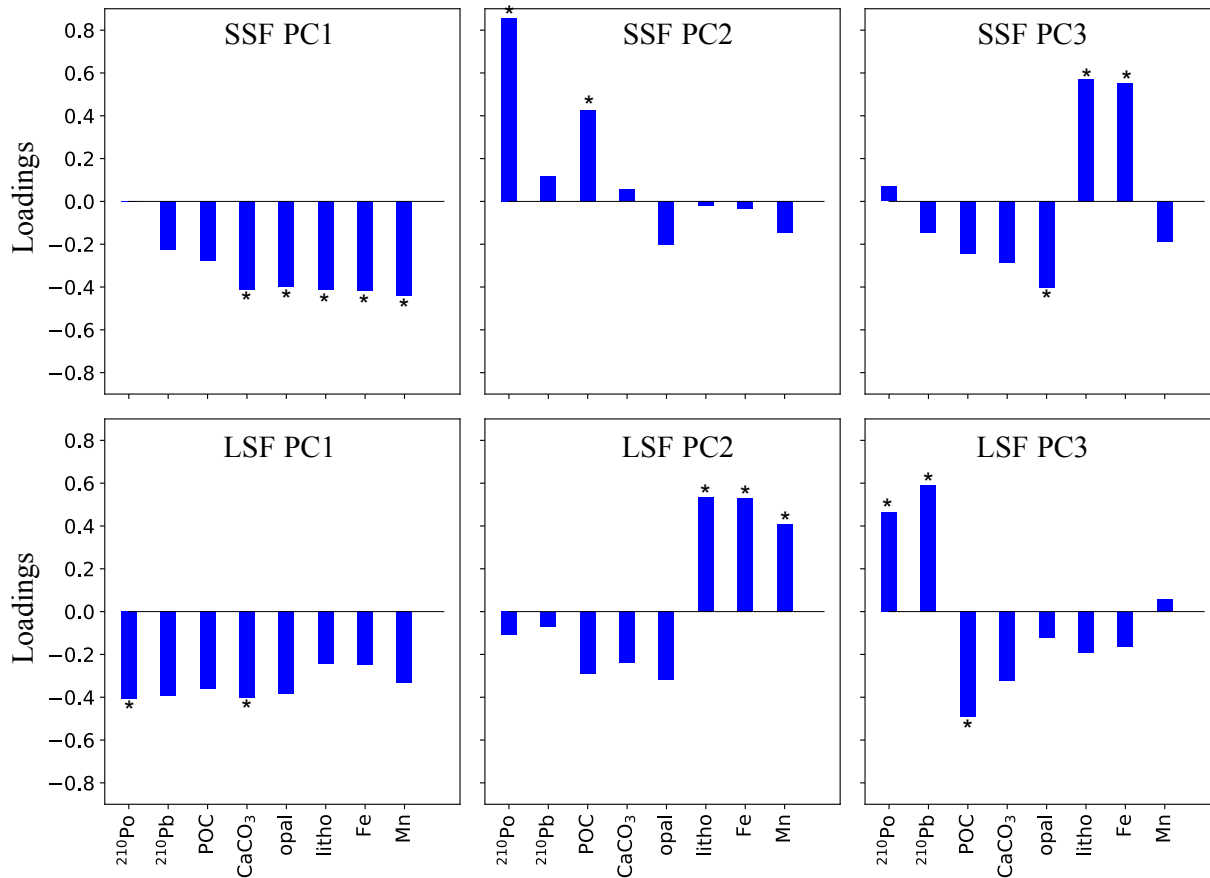243   mainly from ^{210}Po, ^{210}Pb and POC (Table 2, Fig. 2).

244

245
246   Fig. 2. The first three principal component loadings with respect to each variable in the small size fraction (SSF)

247   and the large size fraction (LSF) of the particles. The symbol "*" indicates the absolute loadings that are higher

248   than 0.4.

249

250   Further, PC1 and PC2 scores of the observations for each station were examined and

251   visualized using biplots (Fig. 3). In the SSF dataset, the observations in the open ocean

252   stations generally scored high and positive on PC1, whereas the SSF at coastal station 11-1

253   scored high on PC1 but with negative values. The observations at stn.10-9, on the other hand,

254   had little loading from PC1, but had some variability along PC2, with generally negative

255   scores. Three of the very shallow (~ 40 m) open ocean observations scored relatively high

256   and positive on PC2 (stn.11-12, 11-16, and 11-20) (Fig. 3A). Most observations at stn.10-1

257   scored rather equally on PC1 and PC2, except for one observation (30 m) with significant

258   negative scores on PC1, suggesting this observation was overwhelmingly explained by this
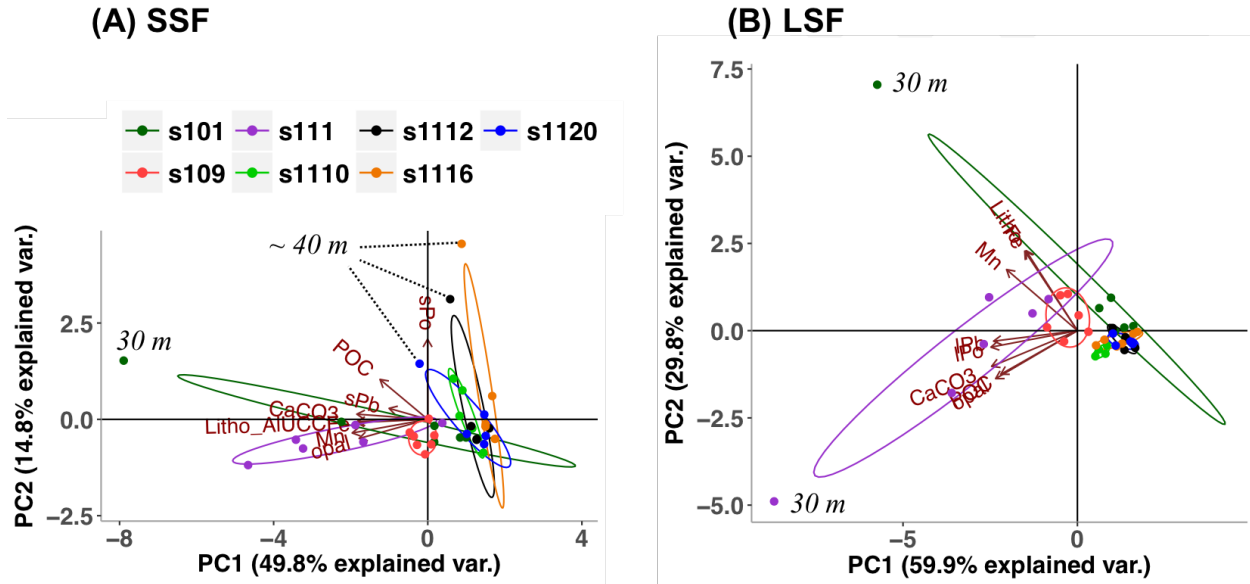259   component.
260

262   Fig. 3. Biplots of principal component (PC1 and PC2) scores based on observations for each station. A: small
263   size fraction (SSF); B: large size fraction (LSF). PC1: first principal component, PC2: second principal
264   component. The color of each point indicates samples from a particular station number, and ovals denote the
265   clustering of those samples. Note that the scales of A and B are different and the depths of the extreme points
266   are annotated (see section 3.2 for detailed description).

267

268   In the LSF dataset, the observations in the open ocean stations mostly scored highly
269   positive on PC1 (Fig. 3B). The PC1 scores for the observations at stn.10-1 were generally
270   higher than PC2 scores (positive), except from the observation at 30 m, which was the only
271   observation from this station to have a strongly negative PC1 score and also had a much
272   higher (positive) score on PC2 compared to the rest of the samples at this station. At stn.10-9,
273   the surface observations had generally negative scores on PC1, and the observations below
274   the surface layer had generally positive scores on PC2. The observations at stn.11-1, on the
275   other hand, scored highly negative on PC1, especially the observation at 30 m.
276   Looking at each biplot (SSF and LSF separately), component scores for the four open
277   ocean stations in both plots displayed a clustered pattern, whereas the observations for the
278   three coastal stations were more varied along PC1 and PC2. Despite the fact that the principal
279   components may represent different causes of variability between SSF and LSF, this suggests

280   more uniform open ocean particle characteristics within each size fraction, but more diverse

281   particle characteristics at the coasts. Additionally, we observed several extremely high scores

282   in a few surface samples (samples annotated on Fig. 3), indicating those observations were

283   overwhelmingly explained by a single component.

3.3. The bulk partition coefficients of ^{210}Po and ^{210}Pb

285   The K_d values for ^{210}Po in the SSF varied between 0.10 and 2.12 $\times 10^7$ L kg^{-1} (median:

286   0.43$\times 10^7$ L kg^{-1}). In contrast, the K_d values for ^{210}Pb ranged from 0.05 to 0.89 $\times 10^7$ L kg^{-1},

287   with a median value half as large as that of ^{210}Po in the SSF (Fig. 4). We also noticed

288   different regional patterns in K_d for both ^{210}Po and ^{210}Pb between the coasts and open ocean.

289   For instance, K_d for ^{210}Po in the SSF in the three stations nearest to the coasts (filled markers)

290   were 2-times lower than those in the remote regions of the ocean (open markers) (Fig. 4A).

291   The K_d(Pb) values, on the other hand, showed higher values between 50 and 150 m near the

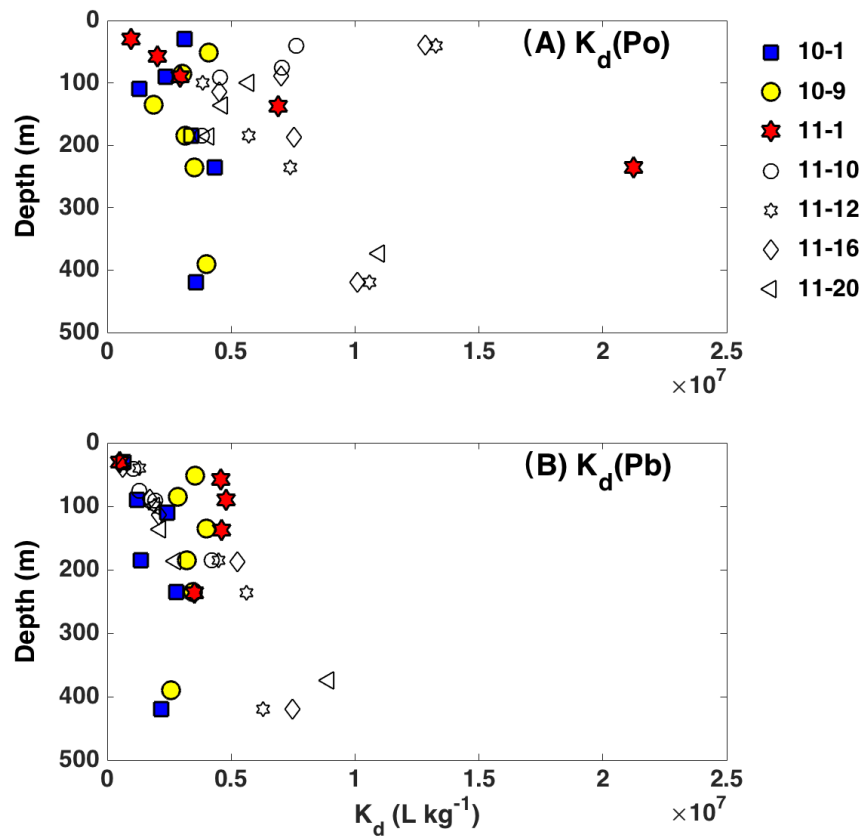292   coastal margins than in the interior ocean (Fig. 4B).

293

Fig. 4. Partition coefficient (K_d in the unit of L kg^{-1}) of ^{210}Po and ^{210}Pb with marine suspended particulate

matter (SPM) in the upper 500 m along the NAZT GA03 transect. (A): K_d of ^{210}Po in the small size

297   fraction (1-51 µm). (B): K_d of ^{210}Pb in the small size fraction. The filled markers indicate the three stations

298   nearest to the margins (stns.10-1, 10-9, 11-1) and the open markers indicate the four open ocean stations

299   (stns.11-10, -12, -16, -20).

300

301   **3.4.Fractionation between ^{210}Po and ^{210}Pb in the bulk samples**

302   The fractionation factor of the bulk sample, F(Po/Pb), which is the ratio of the bulk

303     $K_d(Po)$ to bulk $K_d(Pb)$, ranged from 0.44 to 20.5 in the small particles (Fig. 5). We observed

304   that the fractionation factor generally decreased with depth at nearly all stations, displaying a

305   F(Po/Pb) minimum in the subsurface zone between 100-200 m. For the particles collected

306   from the interior ocean, F(Po/Pb) were all greater than 1 in the upper 300 m, indicating a

307   strong preference for scavenging of ^{210}Po over ^{210}Pb. In contrast, F(Po/Pb) values for

308   particles near the coasts reveal that most were lower than or equal to unity, indicating a slight

309   preference for scavenging of ^{210}Pb over ^{210}Po, or perhaps a higher rate of ^{210}Po

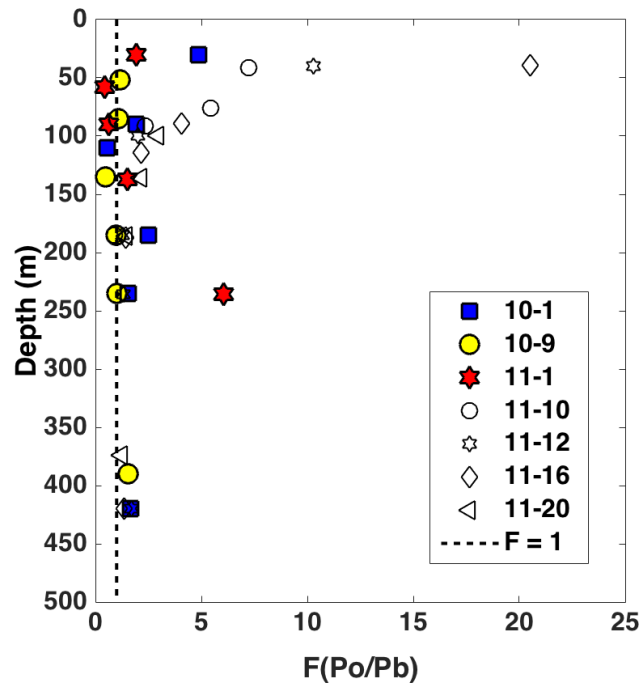310   remineralization from the particles to the seawater (Rigaud et al., 2015).

311

312   Fig. 5. Fractionation of ^{210}Po relative to ^{210}Pb (F(Po/Pb) = $K_d(Po)/K_d(Pb)$) in the small size fraction. The

313   vertical dashed line is drawn for F = 1. The filled markers indicate the three stations nearest to the margins

314   (stns.10-1, 10-9, 11-1) and the open markers indicate the four open ocean stations (stns.11-10, -12, -16, -

315   20).

316

317

4. Discussion

4.1. Correlations of radionuclide activities to chemical composition

We observed correlations between ^{210}Po activity and POC in the large particles across both the coastal and open ocean stations, while similar correlations in the small particles were only found in the open ocean but not in coastal waters (Table 1). When correlations existed between ^{210}Po activity and POC in the upper 500 m, there were also correlations between ^{210}Po activity and CaCO$_3$. In our PCA results, POC and CaCO$_3$ in the large particles had similar loadings on the first three principal components while the loadings of POC and CaCO$_3$ in small particles had similar values on PC1 and PC3, but not on PC2 (Table 2, Fig. 2). These results suggest that POC and CaCO$_3$ were more closely associated with each other and more evenly important to the components in the large particles relative to their relationship in the small particles. Indeed, correlations between POC and CaCO$_3$ were previously observed in the large particles in the upper 2000 m in this section, but no such correlations were seen at any depth in the small particles (Lam et al., 2015). This may be due to a relationship between "ballast" CaCO$_3$ and POC in large, sinking particles (Armstrong et al., 2001).

Despite these relationships in the large particles, in the small particles near the margins no correlation was found between ^{210}Po and POC, while strong positive relationships were observed between ^{210}Po and Fe and lithogenic material (Table 1). As these areas had the highest input of lithogenics (Lam et al., 2015), we suggest that this could reflect scavenging of ^{210}Po by particles from atmospheric dust deposition or continental shelf input. This is an indication that the source of particles can influence the distribution of ^{210}Po, and suggests that the radionuclide activity in the small particles near the coasts has a different relationship with Fe and lithogenic phases than the small particles and large particles in the rest of the study.

While large particles are often aggregates of small particles in the surface ocean, the large particles throughout the water column (top 500m) at the coasts and open ocean had different correlations between the compositional components and ^{210}Po and ^{210}Pb than the small particles, implying that they are not just aggregates of smaller particles. Below the surface layer, there are many reasons to explain why various sized particle compositions could be different (explained further in 4.2).

348   It was reported by Friedrich and Rutgers van der Loeff (2002) that the fractionation of

349   ^{210}Po and ^{210}Pb on particles from the Antarctic Circumpolar Current was dependent on the

350   POC/opal ratio, and suggested that ^{210}Po was more strongly associated with POC while ^{210}Pb

351   was more associated with opal. The Pearson correlation analysis in this study (Table 1)

352   revealed a stronger correlation between POC and ^{210}Po than between POC and ^{210}Pb in

353   general. The results did not show a stronger correlation between opal and ^{210}Pb than between

354   opal and ^{210}Po.

355

356 Fig. 6. The log-log model: $\log F(Po/Pb) = \alpha + \beta \log(\%opal)$ and $\log F(Po/Pb) = \alpha + \beta \log(\%POC)$ was

357 applied to study the linear relationship between the logarithmic transformed dependent and independent

358 variables. Open squares represent log(%POC), and filled triangles indicate log(%opal). The curves were fitted

359 by linear regression functions, and the fitted function and corresponding statistical information are shown in the

360 gray-shaded boxes.

361

362   To examine this further, we applied linear regression models by plotting log(F(Po/Pb))

363   against both log(%POC) and log(%opal) for small particles (Fig. 6). This was done only for

364   small particles because we only calculated $K_d(Po)$ and $K_d(Pb)$ for these particles. A linear

366 function fit the relationship between log(F(Po/Pb)) and log(%opal) reasonably well (R^2 =

367 0.29, n = 35, p = 0.0008), showing a 1% increase in %opal reduces F(Po/Pb) by 0.7%,

368 supporting siliceous matter's preferential affinity for ^{210}Pb. The relationship between

369 log(F(Po/Pb)) and log(%POC), on the other hand, was not well captured with a linear

370 function (R^2 = 0.13, n =35, p = 0.04). Nonetheless, the relationship is still significant,

371 suggesting a 1% increase in %POC increases F(Po/Pb) by 0.8%, supporting the association

372 of ^{210}Po with POC.

373 We did, however, find lower F(Po/Pb) values in surface samples from the coasts than we

374 found in the open ocean, despite the higher POC along the margins (Figure 5). It is worth

375 noting that the phytoplankton composition near the coasts was dominated by siliceous

376 plankton (diatoms, higher %opal) (Twining et al., 2015a), and could result in a decrease in

377 F(Po/Pb), despite high %POC. To further assess this, we applied a multiple linear regression

378 by using both log(%opal) and log(%POC) as predictors and log(F(Po/Pb)) as response:

379 log(F(Po/Pb)) = 0.0155 - 0.63733 log(%opal) + 0.37465 log(%POC) (R^2 = 0.31). The results

380 suggest that %opal has a larger negative impact and %POC had a smaller positive impact on

381 the fractionation. When %opal and %POC are combined in the model, log(%POC) is no

382 longer significant (p = 0.33) while log(%opal) is (p = 0.005). Due to this smaller

383 fractionation between ^{210}Po and ^{210}Pb near the margins, the ^{210}Po deficits with respect to

384 ^{210}Pb were not as significant as those in the subtropical gyre (Rigaud et al., 2015) where non-

385 siliceous organisms like *prymnesiophytes*, *cryptophytes* and *chrysophytes* comprised 40-60%

386 of the community (Twining et al., 2015a).

387 **4.2.Interpretation of PCA**

388 According to the PCA loadings (Fig. 2) and scores in the biplots (Fig. 3), the first

389 principle component (PC1) for both the SSF and the LSF was characterized by similar

390 loadings of the compositional components (all negative) as well as a clear geographic split in

391 sample scores; samples from the open ocean had positive scores, samples from the coastal

392 stations had generally negative scores, and samples from station 10-9 had a unique

393 distribution with both negative and positive scores. Both of these observations suggest a

394 similar interpretation for PC1 for both size fractions. In contrast, the loadings and scores for

395 PC2 were distributed quite differently between SSF and LSF samples, suggesting a different

396 interpretation for this PC in the SSF vs. LSF. In addition, the loadings and scores (data not

397 shown) for PC3 were also distinct between the two size fractions, but there were some

398 similarities between the loadings of PC3 in the SSF and PC2 in the LSF. The loadings for

399 PC2 in the SSF and PC3 in the LSF were relatively distinct from all the other loading

400 patterns.

401   To attempt to interpret the "meaning" of the first three principle components in each size

402 fraction, we plotted the scores of all the samples against physical and chemical characteristics

403 of the samples from the GEOTRACES database. For example, because the scores on PC1 of

404 both size fractions seemed to be related to geographic distribution, but the loadings of all the

405 variables were similar/negative, we expected that some trend other than particulate

406 composition was driving this component from the coast to the open ocean. We hypothesized

407 that this could be related to total suspended particle load (SPM), which tends to be higher at

408 margin stations. Along the transect, between 52 and 99% of the mass of SPM was

409 determined by three biogenic phases: POM (which is $1.88 \times$ POC), opal, and $CaCO_3$ (data

410 not shown), which all are generated by phytoplankton production. Thus, SPM could be used

411 as an indicator of production, with a gradient from the coast to the center of the gyre. Indeed,

412 we observed a strong and significant linear relationship between PC1 scores and the

413 concentration of SPM in both the small and large size fractions (SSF: $R^2 = 0.66$; LSF: $R^2 =$

414 0.73) (Fig. 7A), suggesting a similar interpretation ("production") for PC1 in both size

415 fractions. However, no general pattern was found using SPM as an explanatory variable for

416 the variations in PC2 or PC3 in both size fractions.

417   PC2 has strong positive loadings for both ^{210}Po and POC in the SSF (Table 2, Fig. 2) and

418 we hypothesized that this PC was related to some biogeochemical processes that affected

419 ^{210}Po and POC in a similar manner in the SSF. We did in fact find a strong relationship by

420 using a two-term exponential model ($R^2 = 0.45$) between PC2 in the SSF and apparent

421 oxygen utilization (AOU) (Fig.7B), while none of the other PCs had a significant relationship

422 with AOU. AOU is defined as the difference between the saturation oxygen concentration

423 and the observed oxygen concentration. Dissolved oxygen in the seawater is consumed by

424 microorganisms for the oxidation of organic matter, and therefore AOU can be used as a

425 measure of respiration/remineralization in the oceans (Duteil et al., 2013; Ito et al., 2004).

426 Besides reflecting local respiration/remineralization, AOU is also related to water mass age

427 and the ventilation age of the water (Stanley et al., 2012). This relationship between PC2 in

428 small particles, which has the highest loadings from [210]Po activity, and AOU suggests that

429 recent and past remineralization and respiration affect the [210]Po distribution in small particles
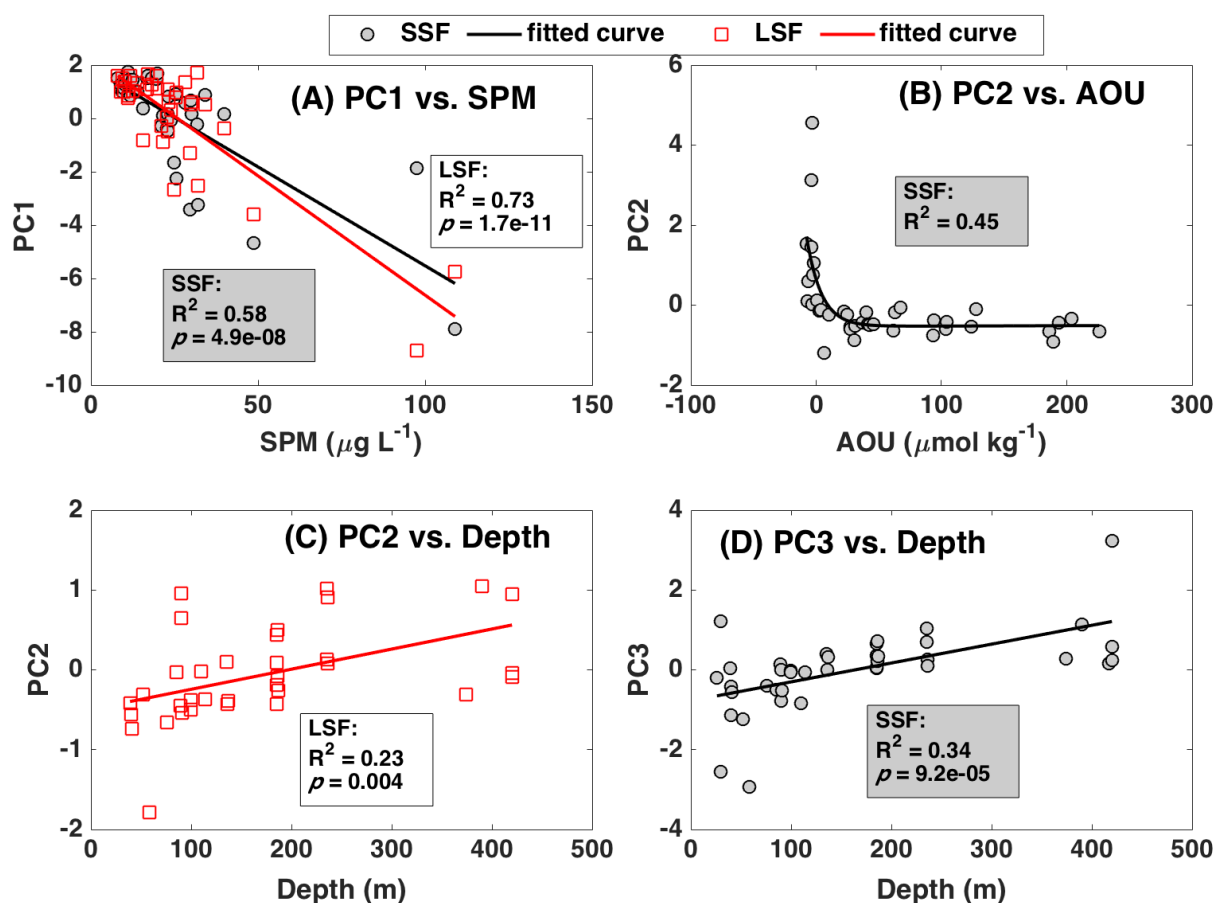
430 more than large particles.

431

432

433 Fig. 7. Relationships between the scores on the first three principal components and the concentration of

434 suspended particulate matter (SPM), apparent oxygen utilization (AOU), and depth. There were a total 9

435 relationships in each size fraction: PC (1, 2, 3) vs. SPM, PC (1, 2, 3) vs. AOU, and PC (1, 2, 3) vs. Depth. Only

436 the graphs with significant relationships are displayed in this figure: (A) PC1 score vs. SPM (SSF and LSF); (B)

437 PC2 score vs. AOU (SSF); (C) PC2 score vs. Depth (LSF); (D) PC3 score vs. Depth (SSF). The filled gray

438 circles represent the SSF and open red squares represent the LSF. The statistical regression lines (solid line) and

439 the R-squared statistic (R^2) are shown in all the plots. The p-value is annotated only for linear regressions (A, C,

440 D) but not for the two-term exponential model (B).

441

442 Looking at the loadings further (Table 2, Fig. 2), it seems that SSF PC3 (12.3% variation

443 explained) and LSF PC2 (29.8% variation explained) could be driven by similar variables,

and appear to reflect a gradient from biogenic particle phases (POC, CaCO$_3$, opal), which have negative loadings, towards abiotic particle phases (litho, Fe, Mn), which have positive loadings. This transition from biogenic material towards inorganic mineral phases tends to occur as freshly-produced particles sink from the surface and degrade with depth. Indeed, when the scores along these principle components were plotted vs. depth, the relationship for both was linear and significant (Fig. 7C and 7D). There were no significant relationships between PC3 and any of the variables we examined in the large size fraction.

The different relationships between principle components and production and remineralization suggests a decoupling of the driving forces that determine composition and ^{210}Po and ^{210}Pb activity in the two size fractions, suggesting both different sources and possibly different residence times between the SSF and the LSF in the top 500m. For example, the source of LSF may reflect production in the surface ocean, especially at the margins where large diatoms, foraminifera, and pteropods could be predominating. The source of SSF in the surface, on the other hand, is probably composed of small diatoms and flagellates. Further differences between the particle characteristics may reflect differences in the residence times of large (faster sinking) and small (slower sinking) particles, especially below the euphotic zone. While there is evidence that large particles are often aggregates of small particles in the surface (Ohnemus and Lam, 2015), there is no reason to expect their compositions will be identical, especially as particles leave the euphotic zone. Small particles at depth may be derived from the disaggregation of larger particles, and may spend several months in the water column as they sink slowly. In contrast, large particles at the same depths could represent fast-sinking material that left the surface within the past several days-weeks, and so may be "fresher" than the small particles in this study due to differences in the extent of degradation and remineralization (Abramson et al., 2010; Wakeham and Canuel, 1988).

Stewart et al. (2007b) applied principal component analysis to explore the connection between ^{210}Po and organic matter within sediment trap particles at 200m in the northwestern Mediterranean. They suggested that degradation contributed the most to the variability in the composition of those sinking particles. While we find remineralization (low AOU as a proxy for "freshness") was an important driver of variation in the small particles, it was not significant for the large particles. The difference in our results, specifically the lack of

475 correlation between AOU and PC scores for large particles, may be caused by differences

476 between the particulate material collected by sediment traps and those collected by in situ

477 pumps (Abramson et al., 2010; Lepore et al., 2009). This concept, however, that degradation

478 and sinking speed can cause some variation of composition within the small and large

479 particles, was confirmed by our result that the depth of the sample is correlated to the

480 distribution along PC2 in the large fraction (which explains 30% of the variation in the

481 particle composition), and along PC3 in the small fraction (12 % of the variation). Thus

482 differences between our results and those of Stewart et al. (2007b) could also be explained by

483 the range of depths of our samples (0-500 m) as opposed to the single depth (200 m) of the

484 sediment trap.

485 **4.3.Particle concentration effect**

486 The K_d values suggest that ^{210}Po has a higher affinity for particles than ^{210}Pb, as its K_d

487 ranged between $10^{6.0}$ and $10^{7.3}$ L kg^{-1} while the K_d values for ^{210}Pb ranged from $10^{5.7}$ to$10^{7.0}$ L

488 kg^{-1}. These K_d values are higher and span a wider range compared to previous values in the

489 nearshore waters off western Taiwan ($10^{5.53}$-$10^{5.56}$ and $10^{5.38}$-$10^{5.87}$ L kg^{-1}, Wei et al., 2012),

490 in surface waters of the northwestern Mediterranean Sea ($10^{5.80}$-$10^{5.97}$ and $10^{4.90}$-$10^{5.08}$ L kg^{-}

491 ^{1},Masqué et al., 2002), and in the turbid waters of the Yellow Sea ($10^{4.59}$-$10^{6.51}$ and $10^{5.23}$-

492 $10^{5.86}$ L kg^{-1}, Hong et al., 1999). All the samples collected in these previous studies were

493 either from surface waters or coastal, turbid environments. The samples evaluated in our

494 study, in contrast, were collected from the surface to 500 m depth, and from the coast to the

495 open ocean, covering a wider range in SPM concentration and more diverse particle

496 composition. Indeed, an even wider range of K_d(Po) values ($10^{4.7}$-$10^{7.2}$ L kg^{-1}) and K_d(Pb)

497 values ($10^{5.0}$-$10^{6.8}$ L kg^{-1}) was observed in a 4000-m water column study in the northern

498 South China Sea (Wei et al., 2014).

499 We examined the effect of particle concentration on the solid/solution partitioning for ^{210}Po

500 and ^{210}Pb by focusing on the uptake of radioactivity from the water to the small particles. The

501 values of partitioning (log K_d) versus particle concentration (log SPM) in the small particles

502 are shown in Fig. 8. Over a range of more than two orders of magnitude of SPM

503 concentrations, an inverse correlation between log K_d and log SPM was observed for both

504 ^{210}Po and ^{210}Pb in this study. Such negative correlation, known as the "particle concentration

505 effect", has been commonly found in field and laboratory observations for ^{210}Po, ^{210}Pb, and

506 other particle-reactive radionuclides such as ^{230}Th, ^{234}Th, ^{231}Pa, and ^{7}Be (Hayes et al., 2015;

507 Wei and Murray, 1994). Although a number of hypotheses have been proposed to explain

508 this observation, the presence of colloidal material which scavenges radionuclides is widely

509 accepted as the factor that results in the particle concentration effect (Honeyman et al., 1988;

510 Honeyman and Santschi, 1989). The colloids provide sorption sites available for particle-

511 reactive species within the operationally defined "dissolved" phase. Increases in particle

512 concentration are associated with increases in the amount of colloidal radionuclides (Benoit

513 and Rozan, 1999). The colloidal radionuclide passes through the 0.45 µm filters and will

514 result in an overestimate of the dissolved radionuclide fraction (A_d) in the water column (Li,

515 2005) as well as lower K_d and hence the inverse relationship between log K_d and log SPM.

516 Recent work on the kinetics of thorium scavenging has suggested that the particle

517 concentration effect could also be explained by a dependency of the loss of thorium from the

518 particle phase (e.g., by desorption and/or remineralization) on particle concentration (Lerner

519 et al., 2017) but it is unknown whether this would also apply to ^{210}Po and ^{210}Pb.   The

520 slope of the log K_d vs. log SPM plot observed for the entire dataset was -0.54 ($R^2 = 0.22$, $p =$

521 0.004, n =35) for ^{210}Po and -0.83 for ^{210}Pb ($R^2 = 0.47$, $p < 0.0001$, n = 35). This finding is

522 comparable with the slope of -0.79 for ^{210}Po and -0.78 for ^{210}Pb in the East China Sea (Su et

523 al., 2016), but the slopes of the regression lines are flatter than the values reported in the

524 water column at Kuala Selangor, Malaysia (-1.05 for ^{210}Po and -1.20 for ^{210}Pb) (Theng and

525 Mohamed, 2005).

526   This relationship was further examined for coastal and open ocean stations respectively,

527 and the results show some regional differences. We found a significant negative relationship

528 between log K_d(Po) and log SPM in the coastal waters ($R^2 = 0.24$, $p = 0.04$), whereas no

529 significant linear correlation was observed in the open ocean (Fig. 8A). In contrast, log

530 K_d(Pb) was significantly correlated with log SPM in the open ocean ($R^2 = 0.91$, $p < 0.0001$)

531 but not at the coastal stations (Fig. 8B). It is also worth noting that the log K_d values for ^{210}Po

532 near the coasts tended to be lower at a given particle concentration (SPM: ~ 10- 25 µg L^{-1})

533 than would have been expected based on the data from the open ocean. In contrast, most log

534 K_d values for ^{210}Pb near the coasts were higher than those observed in the open ocean at the
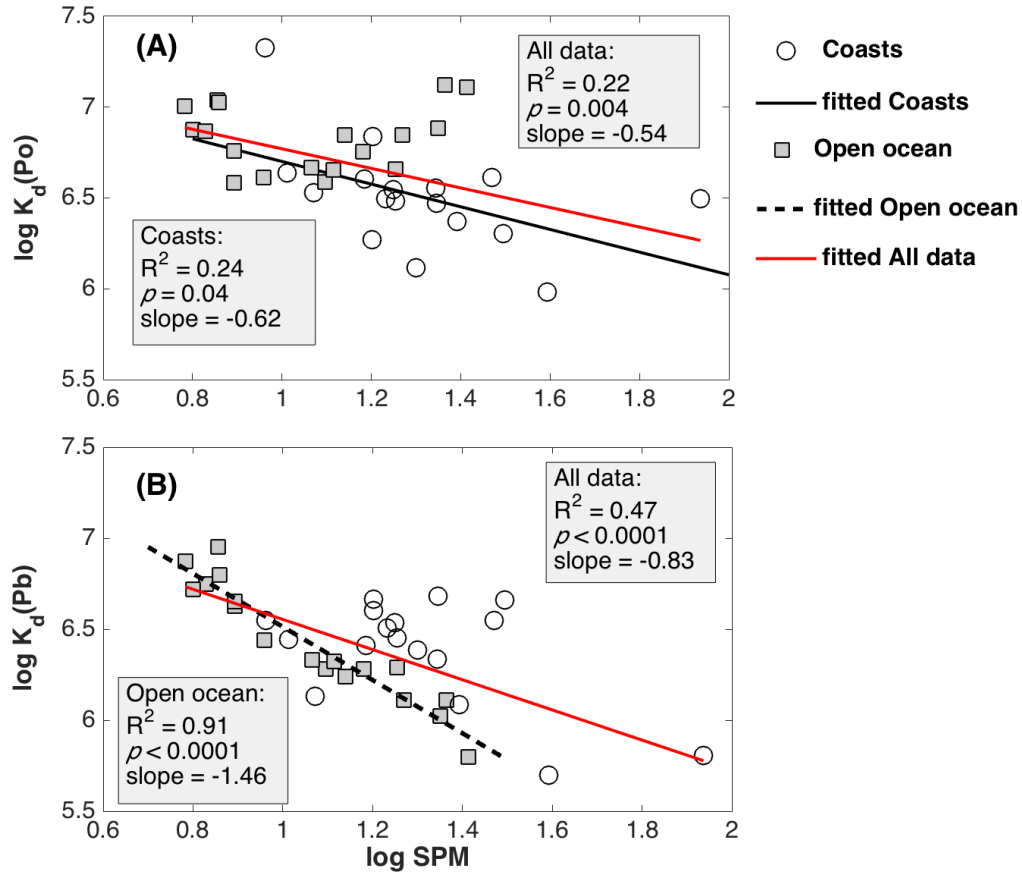
535 same range of particle concentration.

536

Fig. 8. The variation in the solid/solution partitioning (log K_d in L kg^{-1}) for ^{210}Po and ^{210}Pb with particle concentration (log SPM in μg L^{-1}) in the small size fraction from the upper 500 m. (A): log K_d(Po) vs. log SPM. (B): log K_d(Pb) vs. log SPM. The open circles indicate the field data from the three coastal stations (stn.10-1, 10-9, 11-1). The filled squares represent the data from the four open ocean stations (stn.11-10, -12, -16, -20). The black solid line represents the fit to the coastal data, the black dashed line represents the fit to the open ocean data, and the red solid line represents the fit to all data. All slopes shown are significant ($p < 0.05$).

These results suggest that the available binding sites for ^{210}Po and ^{210}Pb for a given particle concentration may be different between the coasts and open ocean along the transect, probably related to particle size, composition, and origin (Balls, 1989; Honeyman et al., 1988). This supports our previous findings in section 4.1, for example, that ^{210}Po and lithogenics were correlated at the coasts but not in the open ocean. Further, the clustering of our PCA scores in Fig. 3 suggests a more homogeneous particle composition in the open ocean and a more heterogeneous particle composition at the coasts, and the relationships between the principal components and proxies for production (SPM) and remineralization (AOU, depth) suggest different drivers for the composition of the particles.

4.4.End-member mixing model evaluation: Observed vs. Predicted

Based on our analyses thus far which indicates a significant difference in the drivers of particle composition along our transect, we separated our proportional composition and bulk K_d (SSF) dataset into coastal (n = 17) and open ocean (n = 14) stations in order to calculate the partition coefficient for each end-member via non-negative least squares regression (Eq. 4). The significant $(K_d)_i$ values for each compositional component obtained from the regression for [210]Po and ^{210}Pb are listed in Table 3.

Table 3. Model-predicted distribution coefficients (L kg^{-1}) for [210]Po ($K_d(Po)_i$) and [210]Pb ($K_d(Pb)_i$) for six end members of particulate materials in the small size fraction (SSF) and their associated fraction factors, F(Po/Pb) = $K_d(Po)/K_d(Pb)$.

	Components	$K_d(Po)$ $\times 10^7$	±	$K_d(Pb)$ $\times 10^7$	±	F(Po/Pb)	±
SSF, Coasts (n = 17)	POM	-	-	-	-	-	-
	CaCO$_3$	1.14	0.29	0.18	0.05	6.3	2.4
	Opal	-	-	3.24	0.35	-	-
	Litho	0.52	0.18	0.3	0.05	1.7	0.7
	Fe	-	-	-	-	-	-
	Mn	46.9	45.9	18.3	12.3	2.6	3.0
SSF, Open Ocean (n = 14)	POM	0.6	0.08	-	-	-	-
	CaCO$_3$	0.5	0.18	-	-	-	-
	Opal	-	-	6.3	1.86	-	-
	Litho	3.7	0.45	3.85	0.16	1.0	0.1
	Fe	2173.6	910.1	322.2	119.1	6.7	3.8
	Mn	-	-	87.3	33.2	-	-

Substituting $(K_d)_i$ values from Table 3 into Eq. 3, we can ultimately obtain the model-predicted K_d value for each sample. Observed K_d vs. predicted K_d (OP) regressions were used to evaluate the six-end member mixing model applied in this study. First, we did OP regressions for the coastal (n = 17) and open-ocean K_d data (n = 14) separately. The analysis of the coefficient of determination (R^2) revealed that 27% of the total variance was explained by the regression model for $K_d(Po)$ at coasts, and 22% in the open ocean (data not shown). In contrast, 57% and 94% of coastal $K_d(Pb)$ and oceanic $K_d(Pb)$ were explained by the OP regression, respectively (data not shown). Then, we applied the OP regressions for the

23

574   combined data (n = 31) from the coasts and open ocean (Fig. 9). The results show 36% of the

575   total variance across all samples was explained by the regression model for $K_d(Po)$ (Fig. 9A),

576   while 85% of the total variance of $K_d(Pb)$ was explained by the regression model (Fig. 9B).

577   The regression of OP values was significant for both $K_d(Po)$ ($p = 0.0003$) and $K_d(Pb)$ ($p =$

578   1.16e-13); the slope of OP for $K_d(Pb)$ was very close to 1 while the slope was further from 1

579   for $K_d(Po)$. The model overestimated observed $K_d(Po)$ at low values and underestimated it at

580   high values. Further, the intercept was significantly different from 0 from the OP regression

581   of $K_d(Po)$ (1.3e+06) while the $K_d(Pb)$ intercept was almost two orders of magnitude smaller

582   (closer to 0). By assessing R^2, the slope, and intercept of the OP regression, we think that the

583   model captured the main characteristics of variability of the observed $K_d(Pb)$ well, while the

584   modeled $K_d(Po)$ values were less reflective of the observed values. In other words, particle

585   composition based on these 6 phases can explain most of the variation in the observed

586     $K_d(Pb)$, but it does not explain variation in the $K_d(Po)$ as well, suggesting either the studied

587   particle composition here is not an important control on $K_d(Po)$ or the model is missing one

588   or more important scavenging end members for [210]Po. This conclusion highlights the caution

589   which must be taken in interpretation of the end-member partition coefficients for [210]Po in

590   the following discussion.
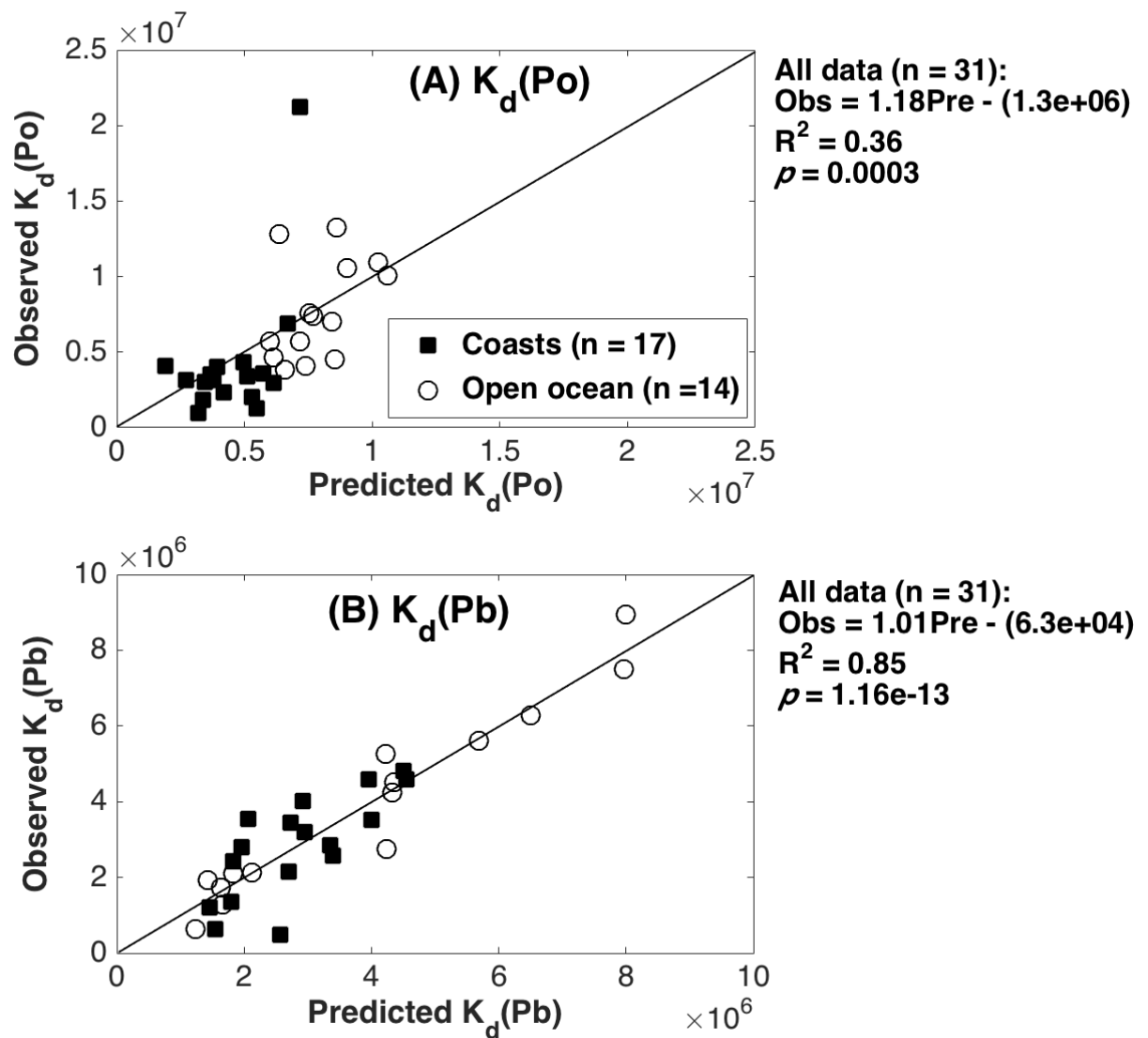
Fig. 9. Observed vs. Model predicted K_d in the small size fraction. (A) $K_d(Po)$; (B) $K_d(Pb)$. The filled squares and open circles represent the coastal data (n = 17) and the open ocean data (n = 14), respectively. The 1:1 line was plotted in each plot, and overall the predication captured the majority of variation in the observed $K_d(Pb)$ while the model overestimated observed $K_d(Po)$ at low values and underestimated it at high values. The statistical results of the regression of observed (Obs) vs. predicted (Pre) K_d values (all data, n = 31) are also shown in the graphs.

4.5. End-member partition coefficients

While we found that the end-member mixing model could predict the overall $K_d(Pb)$ better than the overall $K_d(Po)$, we nevertheless investigated the contribution of each phase's

602   partitioning strength $(K_d)_i$ to the modeled total K_d. As above, we found that the $(K_d)_i$ of each

603   phase differed between the coast and the open ocean (e.g. $K_d(Po)_{Mn}$ for the coast was

604   different than $K_d(Po)_{Mn}$ for the open ocean). Our results are similar to those of Li (2005)

605   wherein the $(K_d)_i$ contribution of four measured components (lithogenic material, organic

606   matter, carbonate, opal) for the total K_d of isotopes of Th, Pa, and Be differed between three

607   oceanic regions. This may reflect multiple influences on $(K_d)_i$ values. The first interpretation

608   of our results is that each measured compositional component (litho, POM, Fe, Mn, opal, and

609   $CaCO_3$) is not chemically identical everywhere along the transect. We mentioned this above

610   when we suggested that there may be different numbers of binding sites for a given

611   composition and concentration of particles in the coast and open ocean.

612   For the lithogenic and organic (POM) components, this may reflect different elemental

613   (e.g. Al vs. Ti vs. Fe for litho, (Ohnemus and Lam, 2015), or P content for POM (Twining et

614   al., 2015b)) or macromolecular (e.g. differences in fatty acid or amino acid content (Stewart

615   et al., 2007b)) composition of these *aggregated* phases from the coast to the open ocean. For

616   the mineral phases, the measured elements (Fe, Mn, Ca, Si) may be consistent from the shore

617   to the center of the gyre, but the organic matrices or biomolecules associated with the

618   minerals could differ. This has been demonstrated in laboratory experiments where the

619   organic biopolymers within mineral matrices can change the sorption nature of those

620   minerals (Chuang et al., 2015; 2013; Yang et al., 2013).

621   Another possible explanation is that partition coefficients are affected by more than

622   particle composition alone. This has been particularly noted in dynamic, coastal

623   environments where physical and chemical conditions vary more than in the open ocean. For

624   example, Turner (1996) highlights salinity affecting trace metal K_d values in multiple

625   estuaries, while Balls (1989) asserts that in European coastal waters particle-particle

626   interactions affect K_d values, justifying the need to include the SPM loadings in the

627   calculation of K_d. That same paper asserts that previous work has found that multiple

628   physiochemical parameters such as salinity and pH influence partition coefficients. These

629   additional factors should be kept in mind as we detail the various $(K_d)_i$ values found for [210]Po

630   and ^{210}Pb below (Table 3).

631   Derived end-member $K_d(Po)_i$ for the six phases were different between the coasts and

632   open ocean. For example, Fe was not a major scavenging phase of [210]Po at the coasts,

whereas it was the most significant scavenger in the open ocean ($10^{10.3}$ L kg^{-1} for ^{210}Po). Mn had the opposite trend; the most significant end-member $K_d(Po)_i$ was derived from Mn at the coasts while no significant $K_d(Po)_i$ value was obtained in the open ocean. Nonetheless, the $K_d(Po)_i$ values for Mn ($10^{8.7}$ L kg^{-1}) and Fe ($10^{10.3}$ L kg^{-1}) at coastal and open ocean stations, respectively, were orders of magnitude above those for the other carrier phases in their associated oceanic regime. Previous laboratory work has also found that MnO_2 and $Fe(OH)_3$ were important in the binding of ^{210}Po (Chuang et al., 2013; Yang et al., 2013; 2015). The $K_d(Po)_i$ values for Fe and Mn reported here, though, are much larger than what has been previously reported (e.g. Fe_2O_3: $10^{4.48}$ L kg^{-1}, MnO_2: $10^{5.19}$ L kg^{-1}) (Yang et al., 2013). The above cited studies, however, did not imply that mineral phases were more important than organic phases. Instead, Chuang et al. (2013) suggested that the direct binding of ^{210}Po to organic biopolymers may be obscured due to the close association between mineral carrier phases and associated biopolymers.

There was no significant $K_d(Po)_i$ value derived for POM at the coasts, while POM was a major scavenging phase of ^{210}Po ($10^{6.8}$ L kg^{-1}) in the open ocean. This was consistent with our previous finding from the pairwise correlations and PCA analyses that there was a significant association between particulate ^{210}Po and POM at the open ocean stations but not at coastal stations. $CaCO_3$ and lithogenics, on the other hand, did not show significant difference between coasts and open ocean, with $K_d(Po)_i$ values for both carrier phases in the range of $10^{6.7}$ – $10^{7.6}$ L kg^{-1} in the two contrasting oceanic regimes.

Derived end-member $K_d(Pb)_i$ values for MnO_2, $CaCO_3$, lithogenics, and POM spanned 2-3 orders of magnitude. We noticed the following relationships for $K_d(Pb)$ in Table 3: K_d (Mn) > K_d (opal) > K_d (lithogenics) > K_d ($CaCO_3$) $\gg$ K_d (Fe) $\approx$ K_d (POM) = 0 at coasts; K_d (Fe) > K_d (Mn) > K_d (opal) > K_d (lithogenics) $\gg$ K_d ($CaCO_3$) $\approx$ K_d (POM) = 0 in the open ocean. The enhanced intensity of scavenging by Mn is consistent with previous work (Canfield et al., 1995; Swarzenski et al., 1999). Both studies concluded that the behavior of ^{210}Pb was tightly coupled to the redox cycling of manganese oxides, but indicated a much less significant role for iron oxides on the behavior of lead. Indeed, laboratory studies showed that MnO_2 had one order of magnitude higher K_d values for ^{210}Pb than Fe_2O_3 (Yang et al., 2013). Nevertheless, the $K_d(Pb)_i$ values for Fe ($10^{9.5}$ L kg^{-1}) and Mn ($10^{8.3-8.9}$ L kg^{-1}) derived here are much larger than what have been determined via experimental studies

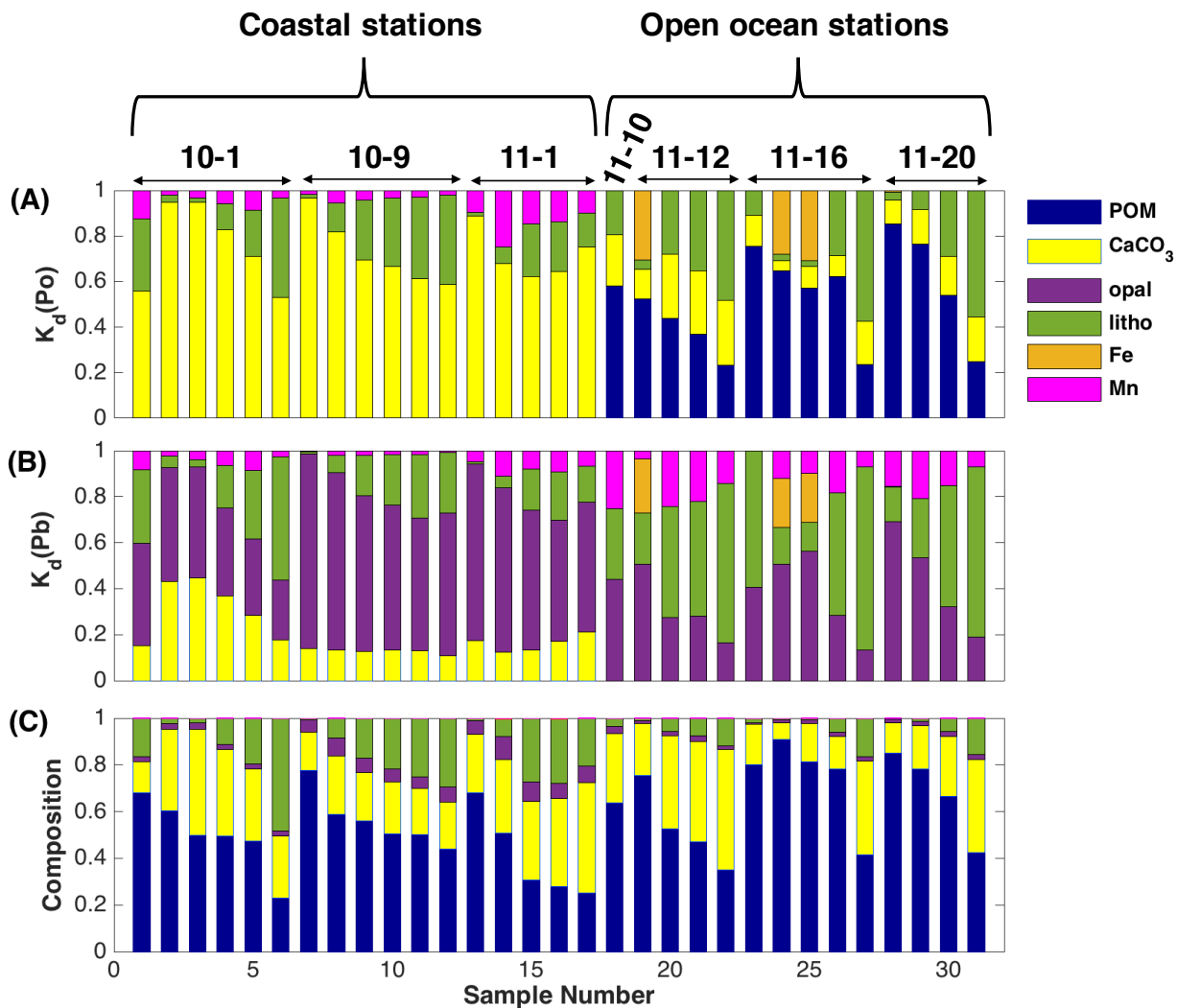| 664 | $(Fe_2O_3: 10^5 \text{ L kg}^{-1}, MnO_2: 10^{6.3} \text{ L kg}^{-1})$ (Yang et al., 2013). This suggests that naturally |
665	formed authigenic MnO_2 may be more reactive in terms of adsorption than the pure phase
666	that has been used in the laboratory studies. Further, the finding that $K_d(Pb)_i$ for Mn was
667	~100 times greater than the compositional partition coefficients for the other components
668	(except Fe in the open ocean) appears consistent with the behavior of ^{230}Th and ^{231}Pa (Hayes
669	et al., 2015), and that of Hg (Lamborg et al., 2016) along the same transect, but the results in
670	those studies were either unexpected or considered a result of methods or operational
671	definitions. Opal appeared to be another major scavenging phase of ^{210}Pb as there were
672	significant $K_d(Pb)_i$ values ($10^{7.5} – 10^{7.8}$ L kg^{-1}) derived for opal from our data set. This
673	finding supports previous work (Friedrich and Rutgers van der Loeff, 2002) and results of
674	this study (Fig. 6), which both suggest an enhanced intensity of scavenging of ^{210}Pb by opal.
675	The modeled fractionation factors (F(Po/Pb)), the ratio of end-member $K_d(Po)_i$ to end-
676	member $K_d(Pb)_i$, ranged from 1 to 6.7 in the small particles (Table 3). The end-member
677	fractionation factors could only be derived when their associated compositional K_d's were
678	available for both ^{210}Po and ^{210}Pb. Thus, we only obtained modeled F(Po/Pb) for $CaCO_3$,
679	lithogenics, and Mn for coastal particles, and for lithogenics and Fe for particles in the open
680	ocean.
681	We further did the OP regression of observed F(Po/Pb) vs. predicted F(Po/Pb) and found
682	it was significant ($R^2 = 0.4$, $p = 0.0001$, data not shown). Even though the predicted $K_d(Po)$
683	values seemed to deviate from the observed $K_d(Po)$ values, the predicted F(Po/Pb) were
684	relatively consistent with observed F(Po/Pb) results. We found that the strongest
685	fractionation between ^{210}Po and ^{210}Pb was associated with coastal $CaCO_3$ (F(Po/Pb) = 6.3)
686	and open ocean Fe (F(Po/Pb) = 6.7) showing a preference for scavenging ^{210}Po by both
687	particulate components. The predicted fractionation factors estimated for lithogenics imply
688	no preference for scavenging ^{210}Po over ^{210}Pb in the open ocean (F = 1), but a weak
689	preference for ^{210}Po over ^{210}Pb at the coasts (F = 1.7).
690	

Fig. 10. The fractional contributions of six end members to the predicted bulk distribution coefficients of A) ^{210}Po (K_d(Po)), and B) ^{210}Pb (K_d(Pb)), in comparison to the weight fractions of the end members in SPM (C) in the upper 500 m. Note that there are two models applied for each K_d: one is based on coastal data (n = 17), the other is open-ocean data (n = 14). The horizontal axis represents the sample number (total 31 samples), ordered from left to right: stn.10-1 (n = 6), 10-9 (n = 6), 11-1 (n = 5), 11-10 (n = 1), 11-12 (n = 4), 11-16 (n = 5), 11-20 (n = 4) (labeled on the top of the plot).

Further, we calculated the percent contribution of each end-member to the bulk distribution coefficients to assess the importance of each end-member to scavenging (end-member K_d for phase i, $(K_d)_i$, multiplied by the percent content of phase i, f_i, divided by the total predicted K_d, $\sum f_i \cdot (K_d)_i$). Fig. 10 summarizes the percent contribution of the six EMs to the predicted partition coefficients of ^{210}Po and ^{210}Pb (Fig. 10A and B, respectively), and

29

704   the weight percent of each end member in SPM (Fig. 10C). At coastal stations, opal was the

705   major contributor (57.1 ± 16.1%) to the predicted K_d(Pb) in the small particles, followed by

706     $CaCO_3$ (20.3 ± 11.1%), lithogenics (17.9 ± 13.8%) and Mn (4.8 ± 3.4%). The major carrier

707   phases of ^{210}Pb in the open ocean, in contrast, were lithogenics (43.5 ±2.0%) and opal (37.8 ±

708   16.8%). Further, Mn and Fe in the open ocean contributed to K_d(Pb) by 14.0 ± 7.8% and 4.8

709   ± 9.4%, respectively (Fig. 10B).

710   The contributions of the carrier phases for [210]Po were also different between the coasts

711   and the open ocean; the major contributor to K_d(Po) was $CaCO_3$ (73.3 ± 14.2%) at coastal

712   stations vs. POM (52.7 ± 20.1%) at open ocean stations. Lithogenics contributed ~ 20% to

713   overall [210]Po scavenging (Fig. 10A). Interestingly, we observed Fe contributing ~ 30% and ~

714   22% in 3 samples (one at stn.11-10, two at stn.11-16) for K_d(Po) and K_d(Pb), respectively,

715   despite the low Fe concentrations of these samples (~ 0.011%). The predicted enhanced

716   scavenging by Mn and Fe for both [210]Po and ^{210}Pb is surprising due to both phases' relative

717   scarcity (low contribution to particle mass). This may highlight a bias in the derived partition

718   coefficients for particle composition which occurs when using weight percentage rather than

719   reactive surface area in the end-member mixing model, as suggested by Hayes et al. (2015)

720   for Th and Pa.

721 **4.6. [210]Po vs. [210]Pb**

722   We observed more significant relationships between [210]Po and POC than between [210]Pb

723   and POC, especially in the open ocean (Table 1). The positive correlation between F(Po/Pb)

724   and %POC suggests the preference for uptake of [210]Po over ^{210}Pb by organic carbon and can

725   be useful in identifying biotic vs. lithogenic particle composition, in the same manner as the

726   ratio of [210]Po/^{210}Pb proposed in Radakovitch et al. (1999). A biological signature

727   (F(Po/Pb) >1) was observed in the upper 50 m at the coastal stations and upper 300 m in the

728   open ocean. On the other hand, F(Po/Pb) values close to or lower than unity at 100 m depth

729   at stn.10-1, at 135 and 185 m at stn.10-9, and at 58 and 90 m at stn.11-1 suggests a more

730   lithogenic composition, such as higher contribution from atmospheric dust or continental

731   margin sediments. Moreover, our end member mixing analysis (EMMA) results show that

732   K_d(Pb) for lithogenics was a factor of three higher than K_d(Pb) for POM (Table 3), further

733   highlighting the important role of lithogenic/inorganic matter in the scavenging of [210]Pb.

734   These results support the well documented preference for [210]Po uptake over ^{210}Pb in marine

organisms and that ^{210}Po is both particle-reactive and bio-reactive, whereas ^{210}Pb is only particle-reactive (Fisher et al., 1983; Heyraud et al., 1976; Heyraud and Cherry, 1979; Larock et al., 1996; Stewart and Fisher, 2003; Wilson et al., 2009). The known bio-reactive behavior of ^{210}Po and its association with sulfur (Balistrieri et al., 1995; Cherrier et al., 1995; Harada et al., 1989), both suggest its cycling in particles is more complicated than ^{210}Pb cycling and supports our hypothesis that important end-members were missing for the model of K_d(Po). The PCA results also support this conclusion because there was a closer association between ^{210}Po and AOU than between ^{210}Pb and AOU, indicating that biological processes affect the cycling of polonium more than that of lead.

An alternative interpretation of the less predictive power of the EMMA for ^{210}Po, the model K_d(Po) values differing from the observed K_d(Po) values, was suggested in the methods when we indicated that the uptake of ^{210}Po by particles is not purely due to adsorption to particle surfaces as is the nature of ^{210}Pb uptake. ^{210}Po can be found associated with particles via three routes: 1) direct sorption of ^{210}Po to particle surfaces, 2) the ingrowth of ^{210}Po from previously sorbed ^{210}Pb, and 3) the bioconcentration and biomagnification of ^{210}Po by organisms. This does not mean that K_d(Po) has no significance, meaning, or use, it may, instead, explain why composition alone could not determine K_d(Po) in this study. It would be nearly impossible to distinguish the relative contribution of these three pathways, but this is an avenue of research that should be pursued. While we cannot easily model the three processes listed above, together they will still result in a higher K_d(Po) than K_d(Pb) for most samples, especially biogenic particles, so the fractionation of the two isotopes can still be used to trace the export of particles.

5. Conclusions

From an investigation into the partitioning of ^{210}Po and ^{210}Pb activity between particles and solution in the upper 500 m water column across the North Atlantic basin, and an analysis of how the particle concentration and composition affect their partitioning, we draw the following conclusions:

(1) While both K_d(Po) and K_d(Pb) were inversely related to particle concentration, their relationships differed between the coasts and open ocean, and the particle concentration effect was strongest for K_d(Pb) in the open ocean.

(2) Our correlation and PCA results indicated that the relationships between ^{210}Po and ^{210}Pb activity and the composition of coastal and open ocean particles were different, but that particle concentration (SPM), remineralization/residence time (AOU), and depth were important drivers of variability in both small and large particles.

(3) A six-end member particle composition mixing model could accurately predict the scavenging of ^{210}Pb, and indicated that opal and lithogenic phases are the major drivers of K_d(Pb). The mixing model could not predict K_d(Po) with as much accuracy, indicating either that the model is missing important scavenging end members for ^{210}Po, (such as sulfur, protein, or another component of organic matter) or that particle composition alone is not the only driver of K_d(Po) because the partitioning of ^{210}Po between the dissolved and particulate phase is more complicated than simple sorption.

(4) Despite the complexity of the cycling of ^{210}Po and ^{210}Pb, and the diversity of particle concentration and composition measured along the GEOTRACES North Atlantic Zonal Transect (GA03), ^{210}Po consistently exhibited a higher affinity for POC than ^{210}Pb, supporting the use of ^{210}Po fractionation and disequilibrium from ^{210}Pb, as a tracer of the export of organic matter in the surface ocean.

References:

Abramson, L., Lee, C., Wakeham, S.G., Szlosek, J., 2010. Exchange between suspended and sinking particles in the northwest Mediterranean as inferred from the organic composition of in situ pump and sediment trap samples. Limnology and Oceanography 55.

Armstrong, R.A., Lee, C., Hedges, J.I., Honjo, S., Wakeham, S.G., 2001. A new, mechanistic model for organic carbon fluxes in the ocean based on the quantitative association of POC with ballast minerals. Deep Sea Research Part II 49, 219–236.

Bacon, M.P., Spencer, D.W., Brewer, P.G., 1976. 210Pb/226Ra and 210Po/210Pb disequilibria in seawater and suspended particulate matter. Earth and Planetary Science Letters 32, 277–296.

Balistrieri, L.S., Murray, J.W., Paul, B., 1995. The geochemical cycling of stable Pb, 210Pb, and 210Po in seasonally anoxic Lake Sammamish, Washington, USA. GCA 59, 4845–4861.

Balls, P.W., 1989. The partition of trace metals between dissolved and particulate phases in european coastal waters: A compilation of field data and comparison with laboratory studies. Netherlands Journal of Sea Research 23, 7–14.

Baskaran, M., Santschi, P.H., 1993. The role of particles and colloids in the transport of radionucldies in coastal environments of Texas. Marine Chemistry 43, 95–114.

Baskaran, M., Santschi, P.H., Benoit, G., Honeyman, B.D., 1992. Scavenging of thorium isotopes by colloids in seawater of the Gulf of Mexico. GCA 56, 3375–3388.

Benoit, G., Rozan, T.F., 1999. The influence of size distribution on the particle concentration effect and trace metal partitioning in rivers. GCA 63, 113–127.

Bibby, T.S., Gorbunov, M.Y., Wyman, K.W., Falkowski, P.G., 2008. Photosynthetic community responses to upwelling in mesoscale eddies in the subtropical North Atlantic and Pacific Oceans. Deep Sea Research Part II 55, 1310–1320.

Buesseler, K.O., Bacon, M.P., Kirk Cochran, J., Livingston, H.D., 1992. Carbon and nitrogen export during the JGOFS North Atlantic Bloom experiment estimated from 234Th: 238U disequilibria. Deep-Sea Research Part A-Oceanographic Research Papers 39, 1115–1137.

Buesseler, K.O., Lamborg, C., Cai, P., Escoube, R., Johnson, R., Pike, S., Masqué, P., McGillicuddy, D., Verdeny, E., 2008. Particle fluxes associated with mesoscale eddies in the Sargasso Sea. Deep Sea Research Part II 55, 1426–1444. doi:10.1016/j.dsr2.2008.02.007

Canfield, D.E., Green, W.J., Nixon, P., 1995. 210Pb and stable lead through the redox transition zone of an Antarctic lake. GCA 59, 2459–2468.

Carvalho, F.P., 2011. Polonium (210Po) and lead (210Pb) in marine organisms and their transfer in marine food chains. International Topical Meeting on Polonium and Radioactive Lead Isotopes 102, 462–472.

Charette, M.A., Moran, S.B., Pike, S.M., Smith, J.N., 2001. Investigating the carbon cycle in the Gulf of Maine using the natural tracer thorium 234. J. Geophys. Res. 106, 11553–11579. doi:10.1029/1999JC000277

Chase, Z., Anderson, R.F., Fleisher, M.Q., Kubik, P.W., 2002. The influence of particle composition and particle flux on scavenging of Th, Pa and Be in the ocean. Earth and Planetary Science Letters 204, 215–229.

Cherrier, J., Burnett, W.C., LaRock, P.A., 1995. Uptake of polonium and sulfur by bacteria. Geomicrobiology Journal 13, 103–115. doi:10.1080/01490459509378009

Chuang, C., Santschi, P.H., Ho, Y., Conte, M.H., Guo, L., Schumann, D., Ayranov, M., Li, Y.,

2013. Role of biopolymers as major carrier phases of Th, Pa, Pb, Po, and Be radionuclides in settling particles from the Atlantic Ocean. Biogeochemistry of trace elements and their isotopes 157, 131–143.

Chuang, C., Santschi, P.H., Jiang, Y., Ho, Y., Quigg, A., Guo, L., Ayranov, M., Schumann, D., 2014. Important role of biomolecules from diatoms in the scavenging of particle-reactive radionuclides of thorium, protactinium, lead, polonium, and beryllium in the ocean: A case study with Phaeodactylum tricornutum. Limnology and Oceanography 59, 1256–1266. doi:10.4319/lo.2014.59.4.1256

Chuang, C., Santschi, P.H., Wen, L., Guo, L., Xu, C., Zhang, S., Jiang, Y., Ho, Y., Schwehr, K.A., Quigg, A., Hung, C., Ayranov, M., Schumann, D., 2015. Binding of Th, Pa, Pb, Po and Be radionuclides to marine colloidal macromolecular organic matter. Biogeochemistry of trace elements and their isotopes 173, 320–329.

Clegg, S.L., Whitfield, M., 1991. A generalied model for the scavenging of trace metals in the open ocean-II. Thorium scavenging. Deep-Sea Research Part A-Oceanographic Research Papers 38, 91–120.

Clegg, S.L., Whitfield, M., 1990. A generalised model for the scavenging of trace metals in the open ocean: I. Particle cycling. Deep-Sea Research Part A-Oceanographic Research Papers 37, 809–832.

Cochran, J.K., 2003. Short-lived U/Th Series Radionuclides in the Ocean: Tracers for Scavenging Rates, Export Fluxes and Particle Dynamics. Reviews in Mineralogy and Geochemistry 52, 461–492. doi:10.2113/0520461

Cutter, G.A., Andersson, P., Codispoti, L., Francois, R., Croot, P., Lohan, M., Obata, H., Rutgers van der Loeff, M.M., 2010. Sampling and Sample-handling Protocols for GEOTRACES Cruises [WWW Document]. URL http://www.geotraces.org/libraries/documents/Intercalibration/Cookbook.pdf (accessed 4.19.16).

Djogic, R., Sipos, L., Branica, M., 1986. Characterization of uranium(V1) in seawater. Limnology and Oceanography 31, 1122–1131. doi:10.4319/lo.1986.31.5.1122

Duteil, O., Koeve, W., Oschlies, A., Bianchi, D., Galbraith, E., Kriest, I., Matear, R., 2013. A novel estimate of ocean oxygen utilisation points to a reduced rate of respiration in the ocean interior. BG 10, 7723–7738.

Efron, B., Stein, C., 1981. The Jackknife estimate of variance. The Annals of Statistics 9, 586–596.

Fisher, N.S., Burns, K.A., Cherry, R.D., Heyraud, M., 1983. Accumulation and cellular distribution of ^{241}Am, ^{210}Po and ^{210}Pb in two marine algae. Marine Ecology Progress Series 11, 233–237.

Friedrich, J, Rutgers van der Loeff, M.M., 2002. A two-tracer (210Po–234Th) approach to distinguish organic carbon and biogenic silica export flux in the Antarctic Circumpolar Current. Deep Sea Research Part I: Oceanographic Research Papers 49, 101–120.

Harada, K., Burnett, W.C., LaRock, P.A., Cowart, J.B., 1989. Polonium in Florida groundwater and its possible relationship to the sulfur cycle and bacteria. GCA 53, 143–150.

Hayes, C.T., Anderson, R.F., Fleisher, M.Q., Vivancos, S.M., Lam, P.J., Ohnemus, D.C., Huang, K., Robinson, L.F., Lu, Y., Cheng, H., Edwards, R.L., Moran, S.B., 2015. Intensity of Th and Pa scavenging partitioned by particle chemistry in the North Atlantic Ocean. Biogeochemistry of trace elements and their isotopes 170 IS -, 49–60.

Heyraud, M., Cherry, R.D., 1979. Polonium-210 and lead-210 in marine food chains. Mar. Biol.

52, 227–236. doi:10.1007/BF00398136

Heyraud, M., Fowler, S.W., Beasley, T.M., Cherry, R.D., 1976. Polonium-210 in euphausiids: A detailed study. Mar. Biol. 34, 127–136. doi:10.1007/BF00390754

Honeyman, B.D., Balistrieri, L.S., Murray, J.W., 1988. Oceanic trace metal scavenging: the importance of particle concentration. Deep-Sea Research Part A-Oceanographic Research Papers 35, 227–246.

Honeyman, B.D., Santschi, P.H., 1989. A Brownian-pumping model for oceanic trace metal scavenging: Evidence from Th isotopes. Journal of Marine Research 47, 951–992. doi:10.1357/002224089785076091

Hong, G.-H., Park, S.-K., Baskaran, M., Kim, S.-H., Chung, C.-S., Lee, S.-H., 1999. Lead-210 and polonium-210 in the winter well-mixed turbid waters in the mouth of the Yellow Sea. Continental Shelf Research 19, 1049–1064. doi:10.1016/S0278-4343(99)00011-4

Ito, T., Follows, M.J., Boyle, E.A., 2004. Is AOU a good measure of respiration in the oceans? Geophysical Research Letters 31, n/a–n/a. doi:10.1029/2004GL020900

Kharkar, D.P., Tiiomson, J., Turekian, K.K., Forster, W.O., 1976. Uranium and thorium decay series nuclides in plankton from the Caribbean. Limnology and Oceanography 21, 294–299. doi:10.4319/lo.1976.21.2.0294

Kohler, U., Luniak, M., 2005. Data inspection using biplots. Stata Journal 5, 208–223.

Lam, P.J., Ohnemus, D.C., Auro, M.E., 2015. Size-fractionated major particle composition and concentrations from the US GEOTRACES North Atlantic Zonal Transect. Deep Sea Research Part II 116, 303–320. doi:10.1016/j.dsr2.2014.11.020

Lamborg, C.H., Hammerschmidt, C.R., Bowman, K.L., 2016. An examination of the role of particles in oceanic mercury cycling. Phil. Trans. R. Soc. A 374, 20150297. doi:10.1098/rsta.2015.0297

Larock, P., Hyun, J.H., Boutelle, S., Burnett, W.C., Hull, C.D., 1996. Bacterial mobilization of polonium. GCA 60, 4321–4328.

Le Moigne, F.A.C., Villa-Alfageme, M., Sanders, R.J., Marsay, C., Henson, S., García-Tenorio, R., 2013. Export of organic carbon and biominerals derived from 234Th and 210Po at the Porcupine Abyssal Plain. Deep Sea Research Part I: Oceanographic Research Papers 72, 88–101.

Lepore, K., Moran, S.B., Burd, A.B., Jackson, G.A., Smith, J.N., Kelly, R.P., Kaberi, H., Stavrakakis, S., Assimakopoulou, G., 2009. Sediment trap and in-situ pump size-fractionated POC/234Th ratios in the Mediterranean Sea and Northwest Atlantic: Implications for POC export. Deep Sea Research Part I: Oceanographic Research Papers 56, 599–613.

Lerner, P., Marchal, O., Lam, P.J., Buesseler, K., Charette, M., 2017. Kinetics of thorium and particle cycling along the U.S. GEOTRACES North Atlantic Transect. Deep Sea Research Part I: Oceanographic Research Papers. doi:10.1016/j.dsr.2017.05.003

Li, Y., 2005. Controversy over the relationship between major components of sediment-trap materials and the bulk distribution coefficients of 230Th, 231Pa, and 10Be. Earth and Planetary Science Letters 233, 1–7.

Masqué, P., Sanchez-Cabeza, J.A., Bruach, J.M., Palacios, E., Canals, M., 2002. Balance and residence times of 210Pb and 210Po in surface waters of the northwestern Mediterranean Sea. Continental Shelf Research 22, 2127–2146. doi:10.1016/S0278-4343(02)00074-2

Murray, J.W., Paul, B., Dunne, J.P., Chapin, T., 2005. 234Th, 210Pb, 210Po and stable Pb in the central equatorial Pacific: Tracers for particle cycling. Deep Sea Research Part I: Oceanographic Research Papers 52, 2109–2139.

Nozaki, Y., Dobashi, F., Kato, Y., Yamamoto, Y., 1998. Distribution of Ra isotopes and the 210Pb and 210Po balance in surface seawaters of the mid Northern Hemisphere. Deep Sea Research Part I: Oceanographic Research Papers 45, 1263–1284. doi:10.1016/S0967-0637(98)00016-8

Ohnemus, D.C., Lam, P.J., 2015. Cycling of lithogenic marine particles in the US GEOTRACES North Atlantic transect. Deep Sea Research Part II 116, 283–302. doi:10.1016/j.dsr2.2014.11.019

Quigley, M.S., Santschi, P.H., Hung, C., Guo, L., Honeyman, B.D., 2002. Importance of acid polysaccharides for 234Th complexation to marine organic matter. Limnology and Oceanography 47, 367–377. doi:10.4319/lo.2002.47.2.0367

Radakovitch, O., Cherry, R.D., Heussner, S., 1999. 210Pb and 210Po: tracers of particle transfer on the Rhône continental margin (NW Mediterranean). Deep Sea Research Part I: Oceanographic Research Papers 46, 1539–1563.

Rigaud, S., Stewart, G., Baskaran, M., Marsan, D., Church, T., 2015. 210Po and 210Pb distribution, dissolved-particulate exchange rates, and particulate export along the North Atlantic US GEOTRACES GA03 section. Deep Sea Research Part II 116, 60–78. doi:10.1016/j.dsr2.2014.11.003

Savoye, N., Benitez-Nelson, C., Burd, A.B., Cochran, J.K., Charette, M., Buesseler, K.O., Jackson, G.A., Roy-Barman, M., Schmidt, S., Elskens, M., 2006. 234Th sorption and export models in the water column: A review. Biogeochemistry of trace elements and their isotopes 100, 234–249.

Shannon, L.V., Cherry, R.D., Orren, M.J., 1970. Polonium-210 and lead-210 in the marine environment. GCA 34, 701–711.

Shimmield, G.B., Ritchie, G.D., Fileman, T.W., 1995. The impact of marginal ice zone processes on the distribution of 21OPb, 21OPo and 234Th and implications for new production in the Bellingshausen Sea, Antarctica. Deep Sea Research Part II 42, 1313–1335.

Stanley, R.H.R., Doney, S.C., Jenkins, W.J., Lott, D.E.I., 2012. Apparent oxygen utilization rates calculated from tritium and helium-3 profiles at the Bermuda Atlantic Time-series Study site. Biogeosciences 9, 1969–1983.

Stewart, G., Cochran, J.K., Miquel, J.C., Masqué, P., Szlosek, J., Rodriguez y Baena, A.M., Fowler, S.W., Gasser, B., Hirschberg, D.J., 2007a. Comparing POC export from 234Th/238U and 210Po/210Pb disequilibria with estimates from sediment traps in the northwest Mediterranean. Deep Sea Research Part I: Oceanographic Research Papers 54, 1549–1570. doi:10.1016/j.dsr.2007.06.005

Stewart, G., Kirk Cochran, J., Xue, J., Lee, C., Wakeham, S.G., Armstrong, R.A., Masqué, P., Carlos Miquel, J., 2007b. Exploring the connection between 210Po and organic matter in the northwestern Mediterranean. Deep Sea Research Part I: Oceanographic Research Papers 54, 415–427. doi:10.1016/j.dsr.2006.12.006

Stewart, G.M., Fisher, N.S., 2003. Bioaccumulation of polonium-210 in marine copepods. Limnology and Oceanography 48, 2011–2019. doi:10.4319/lo.2003.48.5.2011

Stewart, G.M., Fowler, S.W., Teyssié, J.L., Cotret, O., Cochran, J.K., Fisher, N.S., 2005. Contrasting transfer of polonium-210 and lead-210 across three trophic levels in marine plankton. Marine Ecology Progress Series 290, 27–33. doi:10.3354/meps290027

Su, K., Du, J., Baskaran, M., Zhang, J., 2016. 210Po and 210Pb disequilibrium at the PN section in the East China Sea. International Topical Meeting on Polonium and Radioactive Lead Isotopes.

Swarzenski, P.W., McKee, B.A., Sørensen, K., Todd, J.F., 1999. 210Pb and 210Po, manganese and iron cycling across the O2/H2S interface of a permanently anoxic fjord: Framvaren, Norway. Biogeochemistry of trace elements and their isotopes 67, 199–217.

Theng, T.L., Mohamed, C.A.R., 2005. Activities of 210Po and 210Pb in the water column at Kuala Selangor, Malaysia. International Topical Meeting on Polonium and Radioactive Lead Isotopes 80, 273–286.

Turner, A., 1996. Trace-metal partitioning in estuaries: importance of salinity and particle concentration. Biogeochemistry of trace elements and their isotopes 54, 27–39.

Twining, B.S., Rauschenberg, S., Morton, P.L., Vogt, S., 2015a. Metal contents of phytoplankton and labile particulate material in the North Atlantic Ocean. Progress in Oceanography 137, 261–283. doi:10.1016/j.pocean.2015.07.001

Twining, B.S., Rauschenberg, S., Morton, P.L., Vogt, S., 2015b. Metal contents of phytoplankton and labile particulate material in the North Atlantic Ocean. Progress in Oceanography 137, 261–283.

Verdeny, E., Masqué, P., Garcia-Orellana, J., Hanfland, C., Kirk Cochran, J., Stewart, G.M., 2009. POC export from ocean surface waters by means of 234Th/238U and 210Po/210Pb disequilibria: A review of the use of two radiotracer pairs. Deep Sea Research Part II 56, 1502–1518. doi:10.1016/j.dsr2.2008.12.018

Verdeny, E., Masqué, P., Maiti, K., Garcia-Orellana, J., Bruach, J.M., Mahaffey, C., Benitez-Nelson, C.R., 2008. Particle export within cyclonic Hawaiian lee eddies derived from 210Pb–210Po disequilibrium. Deep Sea Research Part II: Topical Studies in Oceanography 55, 1461–1472. doi:10.1016/j.dsr2.2008.02.009

Wakeham, S.G., Canuel, E.A., 1988. Organic geochemistry of particulate matter in the eastern tropical North Pacific Ocean: Implications for particle dynamics. Journal of Marine Research 46, 183–213. doi:doi:10.1357/002224088785113748

Wei, C., Lin, S., Wen, L., Sheu, D.D.D., 2012. Geochemical behavior of 210Pb and 210Po in the nearshore waters off western Taiwan. Marine Pollution Bulletin 64, 214–220.

Wei, C., Murray, J.W., 1994. The behavior of scavenged isotopes in marine anoxic environments: 210Pb and 210Po in the water column of the Black Sea. GCA 58, 1795–1811.

Wei, C.L., Yi, M.C., Lin, S.Y., Wen, L.S., Lee, W.H., 2014. Seasonal distributions and fluxes of 210Pb and 210Po in the northern South China Sea. Biogeosciences 11, 6813–6826.

Wilson, R.C., Watts, S.J., Vives i Batlle, J., McDonald, P., 2009. Laboratory and field studies of polonium and plutonium in marine plankton. International Topical Meeting on Polonium and Radioactive Lead Isotopes 100, 665–669.

Yang, W., Guo, L., Chuang, C., Santschi, P.H., Schumann, D., Ayranov, M., 2015. Influence of organic matter on the adsorption of 210Pb, 210Po and 7Be and their fractionation on nanoparticles in seawater. Earth and Planetary Science Letters 423, 193–201.

Yang, W., Guo, L., Chuang, C., Schumann, D., Ayranov, M., Santschi, P.H., 2013. Adsorption characteristics of 210Pb, 210Po and 7Be onto micro-particle surfaces and the effects of macromolecular organic compounds. GCA 107, 47–64.